LICENTIATE THESIS

A Study on Structural Cores for Lighweight Steel Sandwiches

Samuel Hammarberg

Solid Mechanics

LULEÅ UNIVERSITY OF TECHNOLOGY

A study on structural cores for lightweight steel sandwiches

Samuel Hammarberg

Division of Mechanics of Solid Materials
Department of Engineering Sciences and Mathematics
Luleå University of Technology
Luleå, Sweden

Licentiate Thesis in Solid Mechanics

Printed by Luleå University of Technology, Graphic Production 2018

ISSN 1402-1757
ISBN 978-91-7790-074-0 (print)
ISBN 978-91-7790-075-7 (pdf)

Luleå 2018

www.ltu.se

Preface

The work presented in this thesis has been carried out within the Solid Mechanics group and the Division of Mechanics of Solid Material, Department of Engineering Sciences and Mathematics at Luleå University of Technology (LTU), Sweden. Economic support is supplied through the Swedish lightweight innovation programme - LIGHTer.

I would like to thank the people who supported me throughout the process of completing this work. First of all I would like to thank my friends and colleagues at the Division of Solid Mechanics in Luleå for such a friendly work environment. In particular, my gratitude is towards my supervisors: Prof. Pär Jonsén, Prof. Mats Oldenburg, Dr. Jörgen Kajberg, and Dr. Göran Lindkvist. I would also like to thank my friend and colleague Simon Larsson, with whom I share my office, for being such a good office mate.

Lastly, I want to thank my family, especially my beloved wife, Kristin, and my son, Eliam. You fill my life with love and joy, thank you for your encouragement. I would also like to thank my mom, dad, and brother for support and encouragement to pursue higher educations.

Abstract

Lightweight materials and structures are essential building blocks for a future with sustainable transportation and automotive industries. Incorporating lightweight materials and structures in today's vehicles, reduces weight and energy consumption while maintaining, or even improving, necessary mechanical properties and behaviors. The environmental footprint can, thereby be reduced through the incorporation of lightweight structures and materials.

Awareness of the negative effects caused by pollution from emissions is ever increasing. Legislation, forced by authorities, drives industries to find better solutions with regard to the environmental impact. For the automotive industry, this implies more effective vehicles with respect to energy consumption. This can be achieved by introducing new, and improve current, methods of turning power into motion. An additional approach is reducing weight of the body in white (BIW) while maintaining crashworthiness to assure passenger safety. In addition to the structural integrity of the BIW, passenger safety is further increased through active safety systems integrated into the modern vehicle. Besides these safety systems, customers are also able to chose from a long list of gadgets to be fitted to the vehicle. As a result, the curb weight of vehicles are increasing, partly due to customer demands. In order to mitigate the increasing weights the BIW must be optimized with respect to weight, while maintaining its structural integrity and crashworthiness. To achieve this, new and innovative materials, geometries and structures are required, where the right material is used in the right place, resulting in a lightweight structure which can replace current configurations.

A variety of approaches is available for achieving lightweight, one of them being the press-hardening method, in which a heated blank is formed and quenched in the same process step. The result of the process is a component with greatly enhanced properties as compared to those of mild steel. Due to the properties of press hardened components they can be used to reduce the weight of the body-in-white. The process also allows for manufacturing of components with tailored properties, allowing optimum material properties in the right place.

The present work aims to investigate, develop and in the end bring forth two types of light weight sandwiches; one intended for crash applications (Type I) and another for stiffness applications (Type II). Furthermore, numerical modeling strategies will be established to predict the final properties. The requirements of reasonable computational time to overcome the complex geometries will be met by so-called homogenization. Type I, based on press hardened boron steel, consists of a perforated core in between two face plates. To evaluate Type I's ability to absorb energy for crash applications a hat profile

geometry is utilized. The aim is to increase the specific energy absorption capacity compared to a solid steel hat profile of equivalent weight. Type II consists of a bidirectionally corrugated steel plate, placed in between two face plates. The geometry of the bidirectionally core requires a large amount of finite elements for precise discretization, causing impractical simulation times. In order to address this, a homogenization approach is suggested.

The results from Type I indicate an increased specific energy absorption capacity, due to the perforated cores in sandwich structures. The energy absorption of such a sandwich was 20% higher as compared to a solid hat profile of equivalent weight, making it an attractive choice for reducing weight while maintaining performance. The results from Type II show that by introducing a homogenization procedure, computational cost is reduced with a maintained accuracy. Validation by experiments were carried out as a sandwich panel was subjected to a three point bend in the laboratory. Numerical and experimental results agreed quite well, showing potential of incorporating such panels into larger structure for stiffness applications.

Thesis

This is a compilation thesis consisting of a synopsis and the following scientific articles:

Paper A:
S. Hammarberg, J, Kajberg, G. Lindkvist och P. Jonsén. Homogenization, Modeling and Evaluation of Stiffness for Bidirectionally Corrugated Cores in Sandwich Panels. *To be submitted*

Paper B:
S. Hammarberg, J, Kajberg, G. Lindkvist och P. Jonsén. Evaluation of Perforated Sandwich Cores for Crash Applications. *To be submitted*

Contents

Synopsis

Chapter 1

Introduction

The background and motivation to the study on lightweight steel sandwiches are given followed by the scientific background. The aim, objectives and limitations on the thesis finalize the chapter.

1.1 Background and motivation

In an effort to reduce greenhouse gases associated with transportation, lightweight vehicle components are necessary. This work, investigates how such lightweight structures can be constructed for applications requiring energy absorption or structural stiffness. Furthermore, in order to introduce lightweight material solutions to, for example, the car industry, it is of great importance that accurate simulation methodologies are available to describe the complex sandwich geometries. The simulation methodologies should be time-efficient to facilitate design optimization regarding weight, stiffness and crashworthiness already in the early product development.

According to the United Nation's Intergovernmental Panel on Climate Change (IPCC) it is feasible that humans influence has been the dominant cause of the observed warming since the mid 20th century (Qin et al., 2014). Furthermore, it was stated that greenhouse gases are a likely contributing factor to these effects. This point of view also seems to be the consensus among climate experts. It has been reported that between 90% to 100% of climate scientists share this consensus (Cook et al., 2016). These observations have forced legislatures to establish laws and regulations aimed at reducing emissions such as greenhouse gases, and strive to achieve a carbon free society. In particular, emissions from greenhouse gases due to road transport is to be reduced by 67% by the year 2050 in order to meet long term goals set by the European Union.

Several approaches are possible for reducing emissions, and a few of these will be presented in the following. Optimizing the traffic signal timing is an approach reducing unnecessary stops and delays in traffic, to keep an optimal speed, where fuel usage and emissions are brought to a minimum (Stevanovic et al., 2009). Increasing engine efficiency and considering renewable fuels are also beneficial with respect to reduced emissions. In

recent years the amount of electrical vehicles and plug-in hybrids has increased exponentially. Such vehicles, together with renewable energy sources, have been reported as promising for reducing emission and obtaining a sustainable transportation structure (Saber et al., 2016). Furthermore, to reduce emissions from road transportation, new materials and structures could also be introduced, allowing a reduced weight of vehicle components while performance is kept intact or even improved. At the same time the components must prove to be cost-effective to manufacture as well as requiring little energy when recycled.

1.2 Scientific background

Legislation forces automotive manufacturers to reduce the environmental impact and to meet these requirements there is a great potential in the development of lightweight components for the vehicle's body in white (BIW). While maintaining performance, such as crashworthiness and structural integrity, sustainability must also be considered with respect to manufacturing processes and recyclability.

The idea of reducing weight of vehicle components has been around for a long time. For instance, in the 1970's press hardening was invented by the former SSAB HardTech, now Gestamp HardTech, and in the 1980's Saab Automobile was the first automotive manufacturer to implement such components into the BIW. In the press hardening process, a blank is heated up to a temperature where its microstructure consists of a single phase namely austenite. At this point the steel exhibits a low yield stress and a ductile behavior. Due to these properties the blank can, with ease, be formed into the desired geometry. During forming, the blank is simultaneously cooled to achieve a martensitic structure. Martensite steel exhibits high yield strength and ultimate tensile strength as compared to austenite. Thus, press hardening is a valuable method for producing lightweight vehicle components while maintaining crashworthiness and structural integrity (Li et al., 2003; Georgiadis et al., 2016). Additionally, the press hardening process allows for manufacturing of tailored properties. This is done by adjusting the thermal history in areas were soft zones are desired, allowing the formation of ferrite (Oldenburg and Lindkvist, 2011).

An alternative approach recieving a lot of attention is components based on fiber reinforced polymers (FRP). Their appeal is derived from their superior properties per unit of mass density, due to their specific strength and specific energy absorption during axial compression, compared to metals and steels. In particular, Grauers et al., 2014 illustrates the properties of such materials during quasi-static crushing, where energy absorption was studied specifically in order to understand the underlying mechanisms. It was shown that the the peak crush force was near the mean crush force which would be a desirable attribute during crash loading to reduce harm done to passengers. Furthermore, delamination was discussed as one of the failure mechanism which must be modeled properly for accurate numerical models. Further reading regarding the crash-worthiness of FRP is available in e.g. Carruthers et al., 1998; Jacob et al., 2002 and Alkbir et al., 2016. In the work by Främby et al., 2017 a modeling approach is suggested to capture initiating and propagating delaminations. In addition to delamination, several other complex fracture

mechanism arise for FRP such as fiber kinking and matrix failure. The benefits compared to metals, are: lower weight, corrosion resistant, non-conductive, and superior specific properties. However, there are drawbacks, such as: more complex manufacturing process, expensive to repair, may exhibit more brittle behavior than metals, more sensitive to temperatures. Thus, it comes down to having the proper material in the right place for a given application.

In addition to selecting materials with suitable thermo-mechanical properties for a given application, the geometrical structure of a component can be altered and optimized in order to achieve desired properties, such as sufficient stiffness. A sandwich structure is a good example, which has been reported to be used as early as 1849 in England (Vinson, 2005). Furthermore, sandwich structures based on plywood were also utilized in aircrafts during World War II. Typically a sandwich consists of two stiff, strong skins separated by a lightweight core. Therefore, the moment of inertia is increased with minor influence on the total weight, thereby creating a structural element which efficiently resists bending and buckling loads (Gibson and Ashby, 1999). These attributes have contributed to an increased use of sandwich structures. Areas in which they are used include satellites, aircraft, ships, automobiles, rail cars, wind energy system, bridge construction and many more (Vinson, 2005). Sandwich structures are also present in nature, such as in the skull of a human or in the wing of a bird.

The mechanical properties of the sandwich are significantly affected by the choice of material in the face and core, as well as their geometries. Generally, some constrain on the minimal stiffness is present in order to avoid failure under a given load. At the same time the sandwich mass should be as small as possible. Thus, an optimization problem can be formulated where the object function is the performance, such as stiffness, and the design variables could be densities and thicknesses for core and face plates. For a sandwich, the choice of a core is crucial because it should be a lightweight material while still possessing sufficient stiffness to maintain distance between face plates. In general, the core of a sandwich can consist of any material or geometric pattern. In the following a hand full of core variants will be discussed.

A solid sandwich core is utilized by the TriBond composite by thyssenkrupp (*thyssenkrupp TriBond composite* 2018), where the core consists of hot rolled hardened manganese boron steel with a tensile strength of 1500 MPa. The face plates consist of cold rolled manganese boron steel with a tensile strength of 500 MPa.

In addition to solid cores, foam cores are commonly used in sandwich structures. The mechanical properties of foam are strongly influenced by the bulk material on which the foam is based on (Gibson and Ashby, 1999). A review of steel foams is found in the work by Smith et al., 2012, where manufacturing processes are presented as well as structural applications and modeling approaches. Further work on steel foam can be found in Park and Nutt, 2000; Szyniszewski, Smith, Arwade, et al., 2012; Szyniszewski, Smith, Hajjar, et al., 2014. In addition to steel foam, a lot of work has been done on aluminum foam, see for instance Sulong et al., 2014; Marsavina et al., 2016, which is a common choice for improving crashworthiness in vehicles (Zhang et al., 2013). In Deshpande and Fleck, 2000 and Reyes et al., 2003 it is shown that such foam is a suitable choice for energy

absorption applications. However, the benefits of a steel foam are the increased strength, specific stiffness, lower raw material costs and higher melting temperatures. Furthermore, steel foams are compatible with steel structures and components, thereby less energy is required during recycling. Other bulk materials are also available, such as polymers, see the work by Lachambre et al., 2013, Weinenborn et al., 2016 and Manjunath Yadav et al., 2017.

Another option for obtaining a lightweight sturcutre is cores based on geometrical patterns. A common choice, found in nature, is honeycomb which consists of prismatic cells which nest together to fill a plane (Gibson and Ashby, 1999). The benefits of using honeycomb cores are their inherent out of plane compression strength and low density, which are desirable properties for sandwich panels. Adopting such cores has been done by Aktay et al., 2008 and Nayak et al., 2013. In Mohr and Wierzbicki, 2005, a sandwich with a perforated core is investigated for crashworthiness. A similar type of sandwich structure is utilized in Zhou, Yu, Shao, Wang, and Tian, 2014 and Zhou, Yu, Shao, Wang, and Zhang, 2016, where it is investigated with respect to flexural dynamics utilized in mechanical structures such as national defense, transportation, and aerospace (Zhou, Yu, Shao, Zhang, et al., 2016).

It should be mentioned that many additional types of cores are available, such as truss cores and web cores. However, these will not be presented in further detail in the present work. The final type of core that will be mentioned is the corrugated core. A corrugated core typically consists of some periodic function dependent on one of the in-plane coordinate axis. Such a core is suited for stiffness applications (Biancolini, 2005; Kress and Winkler, 2010; Xia et al., 2012; Bartolozzi et al., 2013; Marek and Garbowski, 2015). A variation of the corrugated core is utilized in Chomphan and Leekitwattana, 2011, Besse and Mohr, 2012 and Zupan et al., 2003, where bidirectionally corrugated cores are utilized.

The present thesis contributes to the scientific field by suggesting two types of sandwich concepts. Type I consists of two skins separated by a perforated core, similar to what was used by Mohr and Wierzbicki, 2005, suited for energy absorption applications. Weight-saving is achieved by clever placement of the holes. Type II consists of a bidirectionally corrugated core, which is suitable for stiffness applications. Superior stiffness is achieved for panels, with the advantage that the core can be manufactured through continues processes such as mill rolling. Both sandwiches are based on ultra high strength steel (UHSS), namely the boron steel 22MnB5.

1.3 Aim and objective

The present thesis aims to reduce the energy consumption of vehicles by lightweight materials and components, thereby reducing the mass of vehicles. The initial objective of this work is thus, to develop models and methods for lightweight steel sandwich construction. The second objective is to reduce computational time required for predicting elastic stiffness for the geometries of the sandwich cores. The following research question can be formulated: "How should lightweight steel sandwiches be modeled to balance validity

and computational cost?”

1.4 Scope and limitations

The scope of the present thesis is to bring forth lightweight steel sandwich structures, to reduce weight of vehicles and energy consumption. The sandwiches are intended for energy absorption and stiffness applications. These structures are evaluated numerically with respect to stiffness and energy absorption. The scope also includes investigation of homogenization methods to reduce computational time for the complex sandwich core geometries. This thesis is limited to only study two types of sandwich cores. For the homogenization procedure, a limit has been set to only predict structural stiffness. Rate dependency has been neglected for both cores and debonding between face plates and core is not taken into account in the numerical models.

Chapter 2

Sandwich mechanics

Sandwich panels are increasingly used for lightweight applications due to their specific properties, such as bending stiffness to weight ratio. Areas of use range from aerospace applications to the automobile industry. In the present chapter a description of the underlying concepts is presented.

2.1 Sandwich theory

A sandwich structure is a type of composite which typically consists of three layers: two face plates kept apart by a core. The face plates are usually stiff with high tensile strength whereas the core is kept as light as possible while still having enough stiffness to withstand transverse load and shearing to keep the face plates apart. In various applications, structures are subjected to distributed pressure loads, causing a curvature in the beam. In the introductory courses to solid mechanics, one might have the opportunity to study bending of beams subjected to such distributed loads. In order to illustrate the benefits of sandwich structures, such a loading case will used as an example. During such a state of deformation, stress and strain varies linearly through the height of the beam cross section according to Euler-Bernoulli beam theory (Timoshenko, 1983). This illustrated in Figure 2.1 and stated by Equations (2.1) and (2.2):

$$\sigma_{xx} = \frac{M_y z}{I_y} \tag{2.1}$$

$$\epsilon_{xx} = \kappa z \tag{2.2}$$

where the coordinate system is defined in accordance with Figure 2.1. In Equation (2.1), M_y is the bending moment around the y-axis, z is the coordinate along the height of the beam with its origin in the neutral axis, and I_y is the moment of inertia around the y-axis. In Equation (2.2), κ is curvature of the beam. Due to this stress distribution, it is more efficient, with respect to weight, to remove material close to the neutral axis, where the stress approaches zero. This is the case for an I-beam or an H-beam, where the

flange carries the bending moment and the web handle the shear forces, which is also the reason for adopting sandwich beams or panels where possible. Compared to an I-beam, the sandwich structures offers continuous support of the face plates whereas for an I-beam the support of the web is located in the middle. Additionally, a sandwich typically offer higher strength and stiffness to weight ratios than a solid steel I-beam. In the following, the engineering sandwich beam theory will be presented, and the normal stress and shear stress distribution will be presented to illustrate the motivation for adopting sandwich structures. In accordance with the Eurler-Bernoulli beam theory, the strain is written as

$$\epsilon_{xx}(x,z) = -z\frac{d^2w}{dx^2} \tag{2.3}$$

where w is the deflection of the beam. The stress is obtained as

$$\sigma_{xx}(x,z) = \epsilon_{xx}E(z) = -z\frac{d^2w}{dx^2}E(z) \tag{2.4}$$

which is integrated over the area, A, of the cross section in order to obtain the normal force

$$N = \int_A \sigma_{xx} dA \tag{2.5}$$

and the moment can be obtained as

$$M = \int_A z\sigma_{xx} dA. \tag{2.6}$$

Inserting Equation (2.4) into Equation (2.6) the following is obtained

$$M = -\int_A z^2 \frac{d^2w}{dx^2}E(z)dA \tag{2.7}$$

which can be written as

$$M = -D\frac{d^2w}{dx^2} \tag{2.8}$$

where D is the flexural stiffness according Equation (2.9).

$$D = \int_A z^2 E(z) dA \tag{2.9}$$

Inserting Equation (2.8) into Equation 2.4 the following expressions is obtained for the normal stress distribution:

$$\sigma = \frac{EM}{D}z \tag{2.10}$$

In order to derive the shear stress distribution over the height of the sandwich beam, the following is derived in in accordance with Figure 2.2. Equilibrium of the body requires

the sum of the moments to equal zero. Thus, summing the moments around the point A of Figure 2.2 the following is obtained.

$$\begin{aligned} -\sigma_x dy\frac{dy}{2} + \sigma_y dx\frac{dx}{2} + \left(\sigma_x + \frac{\partial \sigma_x}{\partial x}dx\right) dy\frac{dy}{2} - \left(\tau_{xy} + \frac{\partial \tau_{xy}}{\partial x}dx\right) dxdy + \\ + \left(\tau_{yx} + \frac{\partial \tau_{yx}}{\partial y}dy\right) dxdy - \left(\sigma_y + \frac{\partial \sigma_y}{\partial y}dy\right) dx\frac{dx}{2} = 0 \end{aligned} \tag{2.11}$$

By division with $2dxdy$ and let $dx \to 0$ and $dy \to 0$ and the following is obtained.

$$\tau_{yx} = \tau_{xy} \tag{2.12}$$

In a similar manner the force equilibrium in the x-direction is obtained as

$$-\sigma_x dy - \tau_{xy}dx + \left(\sigma_x + \frac{\partial \sigma_x}{\partial x}dx\right) dy \left(\tau_{xy} + \frac{\partial \tau_{yx}}{\partial y}dy\right) dx \tag{2.13}$$

which reduces to

$$\frac{\partial \sigma_x}{\partial x} - \frac{\partial \tau_{xy}}{\partial y} = 0. \tag{2.14}$$

Adopting the coordinate system used for the sandwich beam, Equation (2.14) is rewritten as

$$\tau_{xz} = \int \frac{\partial \sigma_x}{\partial x}dz + C = \int \frac{zE(z)}{D}\frac{dM}{dx}dz + C \tag{2.15}$$

where $\frac{dM}{dx}$ is equal to the shear force, V, and the following is obtained

$$\tau_{xz} = \frac{V}{D}\int zE(z)dz + C \tag{2.16}$$

To solve for the integration constant, C, assume no shear stress is present at the top and bottom of the sandwich. Thus, the following is obtained for the face plate of a sandwich with core height, $2h$, and face plate thickness, f,

$$\tau_{xz}^{fp} = \frac{E^{fp}V}{D}\int_z^{h+f} zdzC = \frac{E^{fp}V}{D}\left[\frac{z^2}{2}\right]_z^{h+f} + C = \frac{E^{fp}V}{2D}\left[(h+f)^2 - z^2\right] + C. \tag{2.17}$$

With the condition that $\tau_{xz} = 0$ when $z = h + f$, $C = 0$, and the following is obtained.

$$\tau_{xz}^{fp}(z = h) = \frac{VE^{fp}(2hf + f^2)}{2D} \tag{2.18}$$

Furthermore, due to continuity in the shear stress distribution the following holds

$$\tau_{xz}^{fp}(z = h) = \tau_{xz}^{c}(z = h) \tag{2.19}$$

The shear stress in the core is obtained as

$$\tau_{xz}^{c} = \frac{E^{c}V}{D}\int_{z}^{h} z dz + C = \frac{VE^{2}}{2D}\left(h^{2} - z^{2}\right) + C \tag{2.20}$$

The integration constant is solved for by the results from Equation (2.18) and Equation (2.19).

$$\begin{aligned} \tau_{xz}(z = h) = \frac{VE^{c}}{2D}\left[h^{2} - h^{2}\right] + C \rightarrow \\ \frac{VE^{fp}(2hf + f^{2})}{2D} = C \end{aligned} \tag{2.21}$$

Equation (2.20) is then rewritten as

$$\tau_{xz}^{c} = \frac{V}{2D}\left[E^{2}\left(h^{2} - z^{2}\right) + E^{fp}(2hf + f^{2})\right] \tag{2.22}$$

The normal stress and shear stress distributions over the height of a cross section for a sandwich are presented in Figure 2.3 and Figure 2.4. From these figures it is found that the largest normal stresses are taken by the face plates and the core handles the transverse shear. Thus, the necessary properties of the layers in a sandwich structure can be identified. The face plates should be stiff and be able to withstand large tension and compression stresses, whereas the core should have enough transverse stiffness to maintain the initial distance set between the face plates. Furthermore, studying the equation describing the normal stress and the shear stress distribution, Equation (2.15) and (2.10), it is found that the maximum stress reduces with an increased cross section height, since a larger area takes up the load. These distributions are presented in Figure 2.3 and 2.4. Furthermore, in addition to a lowered stress the flexural stiffness of the beam increases with a cubical relationship, see Figure 2.5. In the figure, the flexural stiffness is plotted as a function of the core height of the beam.

2.2 Sandwich structures for stiffness and energy absorption

For the present work two sandwich cores are investigated, see Figure 2.6, where the Type I consist of a perforated core and Type II of a bidirectionally corrugated core. The Type I sandwich is investigated for energy absorption applications, due to its out-of-plane stiffness and shear rigidity, whereas the Type II is evaluated in structural stiffness applications.

Manufacturing of the Type I sandwich was carried out by drilling holes in to the core specimen, The core and face plates were then joined by a hot rolling process. It was found that the hot rolling process, had contributed to the forming of grains over the interface between face plates and core, this is presented in Figure 3. Thus a strong bond exists

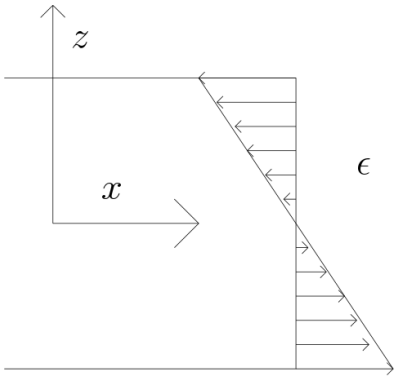

Figure 2.1: Linear strain distribution in a cross section of a beam subjected to an evenly distributed load.

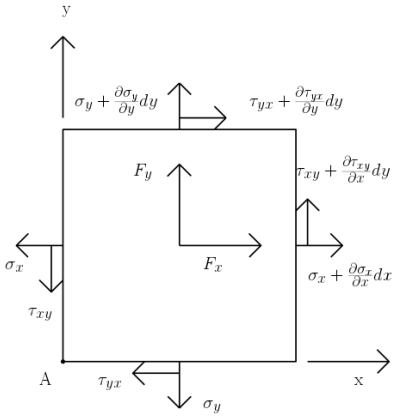

Figure 2.2: 2D stress state in equilibrium.

between the layers of the sandwich. After the hot rolling the geometry of hat profile was obtained by hot stamping.

The Type II sandwich is based on 0.4 millimeters thick boron steel, 22MnB5. The bidirectional geometry of the core is obtained through cold-rolling using patterned rolls. The envelope surfaces of the rolls are are derived from a given sinusoidal function, thus giving the core its desired geometry. Joining between face plates and core is performed by laser welding.

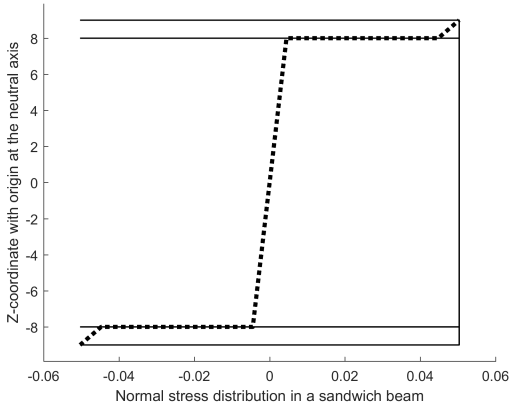

Figure 2.3: Normal stress distribution in a sandwich beam subjected to an evenly distributed load.

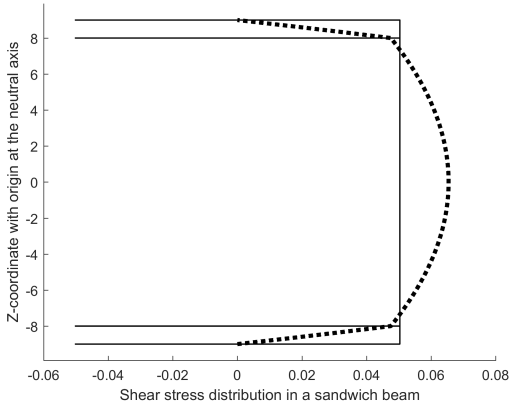

Figure 2.4: Shear distribution in a sandwich beam subjected to an evenly distributed load.

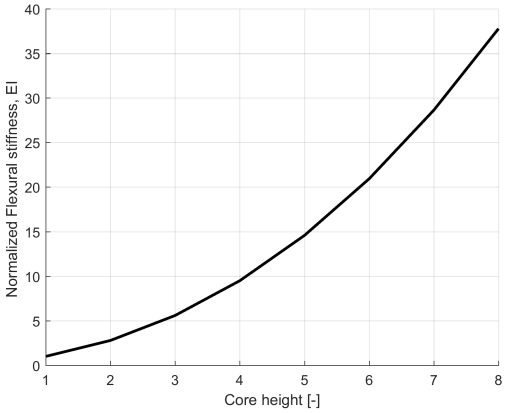

Figure 2.5: Flexural stiffness as function of core height for a sandwich beam.

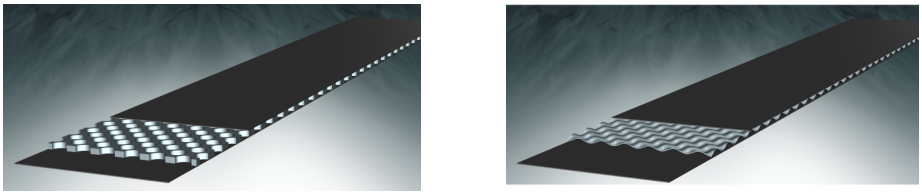

(a) Type I - Perforated core.

(b) Type II - Bidirectionally corrugated core.

Figure 2.6: Sandwich structures based on 22MnB5 steel utilized in the present work.

Chapter 3

Modeling

In order to evaluate the performance of the structures investigated in the present work, the finite element code LS-DYNA has been used. The current chapter aims to give an introduction to the method. In order to emphasize the concept, the finite element formulation is adopted for a one dimensional problem.

3.1 Finite element method

For the present work, the finite element code within the multi-physics solver LS-DYNA was used. LS-DYNA is suitable for analyzing structures subjected to large deformations for static and dynamic loads. Explicit time integration is mainly used, with a possibility to trigger an implicit solution scheme. Contacts are typically handled using a penalty based formulation, where springs are placed between all penetration nodes and contact surfaces. Thus, when two contacting surfaces penetrate, a repulsive force proportional to the distance of penetration is applied.

The finite element method (FEM) is a numerical approach in which physical phenomena, described by differential equations, can be solved in an approximate manner. It should be emphasized that the method is an approximation, and that the results typically contain errors to some degree. If the order of the error is small enough and a sufficient amount of elements is used, the approximated solution of the problem converges toward a true solution.

In engineering, physical phenomena are typically described by differential equations. When the differential equations have been established, a model can be formulated. For the model to be useful in engineering applications, solutions of the differential equations are required. However, it is not uncommon that the particular problem proves to be too complicated to be solved using analytical methods. Thus, some numerical solution scheme can be used to approximate the solution.

When the finite element method is adopted for approximating a solution, the differential equations, describing the physical problem, are assumed to be valid in a given region. This region is then divided into sub-regions, namely finite elements. Thus, a continuum

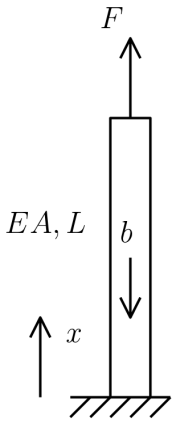

Figure 3.1: Axially loaded bar subjected to a tensile force, F, and its own weight, w. The bar is of length L with area, A, and Young's modulus, E.

with an infinite number of degrees of freedom has been reduced into a region with a finite number of degrees of freedom. For each finite element an approximate solution is then found for the differential equations.

A typical procedure is to first formulate the strong form, which corresponds to the differential equation and its boundary condition. From the strong form the weak form is obtained, which together with the Galerkin method is a basis for the finite element formulation. In order to study this in greater detail the reader is referred to the literature such as Ottosen and Petersson, 1992. However, in the following section the finite element formulation will be derived for a one dimensional bar subjected to an axial load. The displacements obtained from the finite element method will then be compared to an analytical solution.

3.1.1 Axially loaded bar

The current section aims to give the reader an understanding of how the finite element formulation is derived for a one dimensional problem.

Consider the one dimensional, presented in Figure 3.1. The bar is subjected to a tensile force, F, and a body load, b. From the balance of forces and the fundamental relations of solid mechanics, the ordinary differential equation of Equation (3.1) is obtained. It should be noted that E and A correspond to Young's modulus and the area respectively. Furthermore, $u(x)$ is the axial displacement and b the body load acting of the bar due to gravity.

$$EA\frac{d^2u}{dx^2} + b = 0. \tag{3.1}$$

Equation (3.1) is of second order, thus, two boundary conditions are required. The

boundary conditions may either be prescribed forces or displacements at the ends of the bar. For the sake of the example, at $x = L$ the force, F, is known, and at $x = 0$ the displacement, u, is given. The strong form of the axially loaded bar is then given by the differential equation and its boundary conditions.

In order to obtain the weak form, Equation (3.1) is multiplied by an arbitrary weight function, v, and integrated over a region, $0 \leq x \leq L$

$$\int_0^L v \left[EA\frac{d^2u}{dx^2} + b \right] = 0. \tag{3.2}$$

Adopting integration by parts, the following is obtained

$$\int_0^L \frac{dv}{dx} EA \frac{du}{dx} dx = \left[vEA\frac{du}{dx} \right]_0^L + \int_0^L vbdx. \tag{3.3}$$

It should be noted that the first term on the right hand side of Equation (3.3) contains terms related to the end points of the bar, according to the following:

$$\left[vEA\frac{du}{dx} \right]_0^L = vF_{x=L} - vF_{x=0} \tag{3.4}$$

which corresponds to the force applied at the end nodes of the bar. Equation (3.3) is then obtained as

$$\int_0^L \frac{dv}{dx} EA \frac{du}{dx} dx = vF_{x=L} - vF_{x=0} + \int_0^L vbdx. \tag{3.5}$$

In the general case a trial function is chosen to approximate the unknown quantity. Typically, a polynomial to some degree is chosen. For the present case, the unknown corresponds to axial displacement and a linear polynomial is chosen:

$$u \approx \alpha_1 + \alpha_2 x. \tag{3.6}$$

Thus, the shape functions, $\boldsymbol{N}$, for a linear element can be written as

$$\boldsymbol{N} = [-\frac{1}{L}(x - x_j) \ \frac{1}{L}(x - x_i)] \tag{3.7}$$

where x_i and x_j corresponds to the local element nodes. The displacement within an element may then be expressed in terms of the end nodal values, $\boldsymbol{a}$:

$$u = \boldsymbol{N}\boldsymbol{a} \tag{3.8}$$

The derivative of the displacement can now be obtained as

$$\frac{du}{dx} = \frac{d\boldsymbol{N}}{dx}\boldsymbol{a} = \boldsymbol{B}\boldsymbol{a}. \tag{3.9}$$

where $\boldsymbol{B}$ contains the derivatives of the shape function, $\boldsymbol{N}$, according to

$$\boldsymbol{a} = \frac{d\boldsymbol{N}}{dx}. \tag{3.10}$$

Thus Equation (3.3) is rewritten as

$$\left(\int_0^L \frac{dv}{dx} EA\boldsymbol{B} dx\right) \boldsymbol{a} = vF_{x=L} - vF_{x=0} + \int_0^L vb dx. \tag{3.11}$$

A suitable weight function, v, must now be selected. The choice is made in accordance with the Galerkin method, which is a type of weighted residual method. Thus, the weight functions are chosen to be equal to the shape functions, which allows the following reformulation of Equation (3.11)

$$\left(\int_0^L \boldsymbol{B^T} EA\boldsymbol{B} dx\right) \boldsymbol{a} = \boldsymbol{N}F_{x=L} - \boldsymbol{N}F_{x=0} + \int_0^L \boldsymbol{N} b dx. \tag{3.12}$$

where the following can be identified:

$$\boldsymbol{K} = \left(\int_0^L \boldsymbol{B^T} EA\boldsymbol{B} dx\right) \tag{3.13}$$

$$\boldsymbol{f_b} = \boldsymbol{N}F_{x=L} - \boldsymbol{N}F_{x=0} \tag{3.14}$$

$$\boldsymbol{f_l} = \int_0^L \boldsymbol{N} b dx \tag{3.15}$$

and the following can be written

$$\boldsymbol{K a} = \boldsymbol{f_b} + \boldsymbol{f_l}. \tag{3.16}$$

To illustrate how the solution of the finite element converges toward the true solution an analytic solution for the bar of Figure 3.1 is compared to the FEM solution. The bar has the density, ρ, and is subjected to the gravity, g. The obtained analytical expression is presented in Equation 3.17.

$$u(x)_{analytic} = \frac{Fx}{EA} + \frac{\rho g}{E}\left(\frac{x^2}{2} - Lx\right) \tag{3.17}$$

The FEM solution was obtained by discretizing the bar using beam elements, see Figure 3.2, where two bar elements have been used. The figure also illustrates the boundary conditions imposed on the bar. The number of beam elements were increased twice in order to show how the solution is affected, and converged toward the analytic solution. The response from the two methods are presented in Figure 3.3. It is clear that for an increasing number of beam elements, the response from the FEM will converge toward the analytic solution.

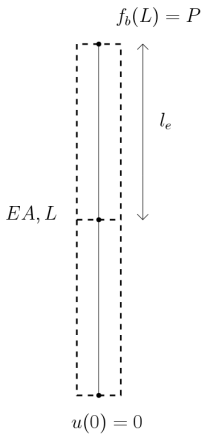

Figure 3.2: Axially loaded bar subjected to a tensile force, F, and its own weight, w. The bar is of length, L with area, A, and Young's modulus, E. The discretization of the bar is also included, where an arbitrary amount of elements has been used. Also, the imposed boundary conditions are displayed.

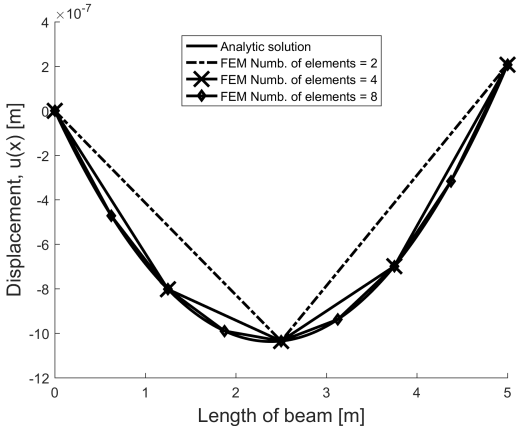

Figure 3.3: The analytical solution of an axially loaded beam is compared to the solution from the FEM. The discretization of the beam was refined twice to illustrate how the approximated displacement converges toward the true solution for an increasing number of elements.

3.1.2 Linear and nonlinear analysis

When the FEM is adopted for analyzing a structure, either a linear or a nonlinear analysis can be performed. The difference between the two is how the stiffness of the structure is handled. The term stiffness refers to the manner in which a structure responds when subjected to a load, which is dependent on the geometrical stiffness, material stiffness, and the stiffness contributed by boundary conditions. When a structure is subjected to loading, the geometry may be distorted and the material may yield. Thus, the stiffness of the structure has been changed and must be updated for the current state. The change in stiffness may also arise from nonlinear boundary conditions and large displacements. However, if the structure is loaded in such a way that the geometrical and material changes are small enough, the stiffness can be assumed to remain constant. This is the case for a linear analysis, which simplifies the problem to be solved. For a nonlinear analysis, the stiffness must be updated during deformation and some numerical solution scheme is required. The nonlinear behavior of materials is captured by selecting a constitutive model which represents the material in a suitable manner (Ottosen and Ristinmaa, 2005; Bonet and Wood, 2008).

3.1.3 Material models

The present section aims to give a brief overview of some of the constitutive models used for material representation. For a more detailed description of the subject, the reader is referred to the litterature, such as Ottosen and Ristinmaa, 2005.

A fundamental necessity before performing a finite element analysis, is selecting a material model. The material model should represent the material in such a way, that physically correct and accurate results are produced when the material is subjected to a load. Thus, when a continuum is subjected to deformation the material of the continuum is strained. Due to the strain state, stresses arise. The manner in which strains and stresses are coupled is handled by the constitutive relation. A variety of such relations is available, such as elasticity, plasticity, visco-elasticity, visco-plasticity, and creep. Furthermore, the material depend on the manner in which the loading is applied, thus some strain rate dependent material model may be required. Furthermore, if plasticity is to be considered, the manner in which the material behaves beyond yielding must then be handled. Thus, it must be made sure that the constitutive model is able to predict what the user wants to study. In the following, material models for capturing the plasticity response will be discussed briefly.

If steel is assumed to behave in a linear elastic manner, Young's modulus, E describes the relation between the stress, σ, and strain, ϵ for a one dimensional case, see Equation (3.18).

$$\sigma = E\epsilon \tag{3.18}$$

If the loading is increased, to such a point that the stress in the material exceeds a given value, the material will experience permanent deformation, namely plastic strains.

The stress level at which this occurs may be called the initial yield stress, σ_{y0}. Beyond the point of σ_{y0}, some further method is required to determine the stress in the material.

A simple approach for handling the stresses beyond σ_{y0}, is to assume the material to be perfect plastic. For such a case, the stress never rises above σ_f, and no further method is required for updating the stress beyond this point.

Alternatively, the material can be approximated to harden linearly. That is, if the stress reaches beyond σ_{y0}, the yield stress will increase as the material is experiencing plastic flow. The yield stress may then be written in the following form

$$\sigma_y = \sigma_{y0} + H \cdot \epsilon^p_{eff}. \tag{3.19}$$

where H is the hardening modulus corresponding to the slope of the hardening curve, and ϵ^p_{eff} is the effective plastic strain.

In addition to perfect plasticity and linear hardening, other types of hardening behavior also exists, such as nonlinear hardening responses, typical for alloyed steel and aluminum, or softening of the material, characteristic for rocks and concrete loaded in compression.

In the general case, a three dimensional stress state will arise in the material when subjected to loading. If linear isotropic elasticity is assumed the following holds true

$$\sigma_{ij} = D_{ijkl}\epsilon_{kl} \tag{3.20}$$

$$D_{ijkl} = 2G\left[\frac{1}{2}\left(\delta_{ik}\delta_{jl} + \delta_{il}\delta_{jk}\right) + \frac{\nu}{1-2\nu}\delta_{ij}\delta_{kl}\right] \tag{3.21}$$

where σ_{ij}, ϵ_{ij}, and D_{ijkl} are the stress, strain and constitutive tensors respectively, and G corresponds to the shear modulus. In order to evaluate if the stress state of Equation (3.20), is yielding, the stress components must be combined in some manner. Typically, some stress invariant is used that can be compared to the yield stress of a material. In general, this yield criterion can be expressed as $F(I_1, J_2, cos3\theta) = 0$, where I_i and J_i are the Cauchy and deviatoric stress invariants respectively. Plastic deformations occurs if $F(I_1, J_2, cos3\theta) > 0$, and I_1, J_2, $cos\theta$ are given as

$$I_1 = \sigma_{kk} \tag{3.22}$$

$$J_2 = \frac{1}{2}s_{ij}s_{ji} \tag{3.23}$$

$$cos3\theta = \frac{3\sqrt{3}}{2}\frac{J_3}{J_2^{3/2}} \tag{3.24}$$

$$J_3 = \frac{1}{3}s_{ij}s_{jk}s_{ki} \tag{3.25}$$

where s_{ij} is the deviatoric stress tensor given by

$$s_{ij} = \sigma_{ij} - \frac{\sigma_{kk}}{3}\delta_{ij}. \tag{3.26}$$

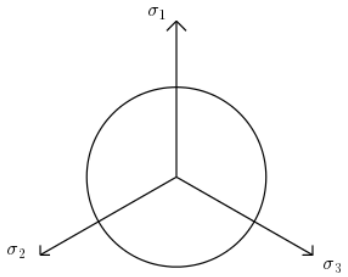

Figure 3.4: von Mises yield surface in the principal stress space, with the view along the hydrostatic axis.

In general, it is possible to distinguish two groups of yield criterion: those that do not depend on the hydrostatic pressure, $I_1/3$ and those who do. The former typically applies to metals and steel, whereas the latter applies to porous material such as concrete, soil and rocks.

A common material model for predicting yield in metals and steels is the von Mises criterion, which is also referred to as J_2-plasticity since its yield function is only expressed in terms of the second deviatoric invariant, J_2, according to Equation (3.27). The von Mises yield surface corresponds to a cylinder in the principal stress space, with its axis of symmetry coinciding with the hydrostatic axis, see Figure 3.4. If $F_{vonMises} \leq 0$ is not fulfilled, the material will yield. For steel, the material may experience isotropic or kinematic hardening. Isotropic hardening indicates that the radius of the yield surface, being a function of the plastic strains, will increase during plastic flow while the origin is fixed. For kinematic hardening, the radius is fixed while the origin is moved during plasticity. If hardening occurs, this will affect the yield surface and some method for updating the yield surface must be utilized. In order to update the yield surface and scale back to stress to fulfill the yield criterion, the radial return method, presented in Schreyer et al., 1979 and Ottosen and Ristinmaa, 2005, is a suitable method. It should also be mentioned that other yield surfaces exist for predicting yield in steels and metals, such as the Tresca criterion which will not be presented in further detail here. However, experiments have shown the von Mises criterion fits experiments well. Thus, the von Mises criterion should preferred over the Tresca criterion.

$$F_{vonMises} = \sqrt{3J_2} - \sigma_{y0} \tag{3.27}$$

A constitutive routine suitable for porous material, such as concrete, soil and rocks, is the Drucker-Prager criterion, presented in Equation (3.28). The criterion is dependent on the deviatoric stress invariant, J_2, and the hydrostatic stress due to the presence of I_1. Furthermore, it should be noted that the expression reduces to Equation (3.27) if $\alpha = 0$. In the principal stress space, the Drucker-Prager yield surface forms a cone, which should be compared to the cylinder obtained for the von Mises yield surface. In addition to the Drucker-Prager criterion, the Coulomb criterion is available for representation of

porous material. This will not be presented further, and the interested reader is referred to Ottosen and Ristinmaa, 2005.

$$F_{Drucker-Prager} = \sqrt{3J_2} + \alpha I_1 - \beta \tag{3.28}$$

Chapter 4

Summary of appended papers

The current chapter contains a summary of the appended papers of the thesis, and the authors contribution is given.

4.1 Paper A

In Paper A, a sandwich structure is presented intended for structural stiffness applications. The sandwich is based on hardened boron steel, with a bidirectionally corrugated core. Due to the complex geometry of the core, a homogenization procedure is proposed in order to reduce computational time. The homogenization procedure is limited to predict structural stiffness. The aim of the paper is to be able to replace current vehicle components with those based on the suggested sandwich structure, thereby reducing weight and energy consumption of vehicles. It was found that the suggested sandwich structure was able to provide stiffness and drastically reduce total weight of the component, as a steel sheet would require to have 2.5 times higher mass than the sandwich, in order to provide equivalent stiffness.

Author contribution: The present author performed the numerical simulations and evaluation against the experimental data, as well as wrote the main part of the paper.

4.2 Paper B

In Paper B, a sandwich structures is presented intended for energy absorption applications. The sandwich is based on hardened boron steel, with a perforated core. In order to numerically evaluate the properties of the sandwich, a hat profile geometry is utilized. The hat profile is subjected to a crushing force in the form of a barrier. From the numerical simulations the force-displacement and energy absorption is evaluated, and compared to a hat profile consisting of a solid steel sheet with the equivalent weight of the sandwich. It was found that the energy absorption ability is approximately 20% increased as

compared to a hat profile consisting of a solid steel sheet.

Author contribution: The present author performed the numerical simulations and wrote the main part of the paper.

Chapter 5

Discussion and conclusions

Due to legislation, the greenhouse gas emissions emitted by vehicles, are forced to be reduced. In order to achieve this, new technologies are required, which provide more energy efficient vehicles. Further improvement, with respect to energy efficiency, is achieved by lowering the weight of vehicle components. Thus, new materials and methods are required for construction of the BIW of vehicle. This thesis intends to contribute to the knowledge of lightweight structures, with respect to construction and numerical modeling for structural stiffness and energy absorption applications.

A sandwich panel with a bidirectionally corrugated core, suitable for stiffness applications, is suggested in Paper A. It is found that the specific stiffness of the sandwich is superior to panels of equivalent stiffness, based on solid steel sheets. This finding agrees with what has been reported in previous work (Bartolozzi et al., 2013). Computational time for predicting structural stiffness is reduced by utilizing a homogenization procedure.

The sandwich of Paper A is suited for integration in vehicle structures, where panels for structural stiffness are required, such as floors and battery boxes in car bodies. Due to the sinusoidal nature of the core, the sandwich is less suited for components formed across a radius. This would cause the wavelength of the core to be increased, reducing the height of the sandwich and thereby its stiffness. The homogenization procedure is limited to predicting structural stiffness, neglecting large deformations and plasticity. This limits where the homogenized sandwich can be placed in a numerical car crash.

Cold-rolling is utilized for producing the panel in Paper A, allowing for an efficient and continuous manufacturing process for large-scale production, keeping costs down.

A sandwich hat profile with a perforated core, evaluated for energy absorption, is studied in Paper B. Mohr and Wierzbicki, 2005 reports using a similar type of sandwich for construction of a crash box, with no increase in the specific energy absorption. Therefore, in Paper B, the hole distribution of the perforated core, is carefully distributed. It is found that the specific energy absorption of the sandwich hat profile is enhanced compared to hat profiles of equivalent weight, based on solid steel sheets.

Manufacturing of the sandwich is carried out by drilling holes in to the core specimen,

according to a specified pattern. The core and face plates are joined by a hot rolling process. It was found that grains formed over the interface between core and face plates, ensuring a strong bond. From Paper B, it could be concluded that the perforated sandwich is suitable for components absorbing energy, such as crash beams of vehicle bodies. Also, manufacturing methods for the perforated core must be investigated further, developing efficient and cost-effective processes for large-scale production.

Furthermore, the nature of the perforated core requires a large number of finite elements for discretization, causing long simulation times. A homogenization method is thus required which reduces the amount of elements while maintaining desired accuracy for crash simulations. This issue is not dealt with in Paper B.

Chapter 6

Outlook

According Section 1.4, the homogenization procedure was limited to only being able to predict elastic structural stiffness for small deformations. Future work involves studying homogenization procedure able to predict the response during large deformations and plasticity for both types of cores. Such a procedure is necessary if components based on the suggested structures are to be used in vehicle structures, to keep simulation time down. Thus, a future aim is to represent both the skins of the sandwich and the core with a single solid and/or shell element. This applies to the sandwich structures of both Paper A and Paper B.

The papers presented in this thesis, only deal with the numerical simulations of already manufactured products, and not the manufacturing process itself. To base components on the Type I sandwich structure, a feasible manufacturing process must be established, allowing for cost-effective production. Numerical models of manufacturing is also necessary in order to be able optimize the properties of the end product. Future work also involves studying how the wavelengths of the Type II sandwich should be modified and manufactured, in order to allow forming of components with bidirectionally corrugated cores.

Furthermore, numerical models for predicting fatigue for the sandwich structures of Paper A and Paper B is also to be investigated. This is of importance if the sandwich structures are to be incorporated into the bodies of heavy duty vehicles.

References

Aktay, L., A.F. Johnson, and B.H. Kröplin (2008). Numerical modelling of honeycomb core crush behaviour. *Engineering Fracture Mechanics* 75.9, pp. 2616–2630.

Alkbir, M.F.M., S.M. Sapuan, A.A. Nuraini, and M.R. Ishak (2016). Fibre properties and crashworthiness parameters of natural fibre-reinforced composite structure: A literature review. *Composite Structures* 148, pp. 59–73.

Bartolozzi, G., M. Pierini, U. Orrenius, and N. Baldanzini (2013). An equivalent material formulation for sinusoidal corrugated cores of structural sandwich panels. *Composite Structures* 100, pp. 173–185.

Besse, C.C. and D. Mohr (2012). Optimization of the Effective Shear Properties of a Bidirectionally Corrugated Sandwich Core Structure. *Journal of Applied Mechanics* 80.1, p. 011012.

Biancolini, M.E. (2005). Evaluation of equivalent stiffness properties of corrugated board. *Composite Structures* 69.3, pp. 322–328.

Bonet, J. and R.D. Wood (2008). *Nonlinear continuum mechanics for finite element analysis*. Cambridge University Press, p. 318.

Carruthers, J.J., A.P. Kettle, and A.M. Robinson (1998). Energy absorption capability and crashworthiness of composite material structures: A review. *Applied Mechanics Reviews* 51.10, p. 635.

Chomphan, S. and M. Leekitwattana (2011). Finite Element Study of the Stress Response of Bi-Directional Corrugated-Strip Core Sandwich Beam Suphattharachai Chomphan and 2 Manit Leekitwattana Department of Electrical Engineering , Faculty of Engineering at Si Racha , Department of Naval Architectu. 7.9, pp. 1335–1337.

Cook, J., N. Oreskes, P.T. Doran, W.R.L. Anderegg, B. Verheggen, E.W. Maibach, J.S. Carlton, S. Lewandowsky, A.G. Skuce, S.A. Green, D. Nuccitelli, P. Jacobs, M. Richardson, B. Winkler, R. Painting, and K. Rice (2016). Consensus on consensus: a synthesis of consensus estimates on human-caused global warming. *Environ. Res. Lett* 11.

Deshpande, V.S. and N.A. Fleck (2000). Isotropic constitutive models for metallic foams. *Journal of the Mechanics and Physics of Solids* 48.6, pp. 1253–1283.

Främby, J., M. Fagerström, and J. Brouzoulis (2017). Adaptive modelling of delamination initiation and propagation using an equivalent single-layer shell approach. *International Journal for Numerical Methods in Engineering* 112.8, pp. 882–908.

Georgiadis, G., A.E. Tekkaya, P. Weigert, S. Horneber, and P. Aliaga Kuhnle (2016). Formability analysis of thin press hardening steel sheets under isothermal and non-isothermal conditions.

Gibson, L. and M. Ashby (1999). *Cellular Solids - Structure and Properties - Second edition*. 2nd. Cambridge University Press (2nd edition).

Grauers, L., R. Olsson, and R. Gutkin (2014). Energy absorption and damage mechanisms in progressive crushing of corrugated NCF laminates: Fractographic analysis. *Composite Structures* 110.1, pp. 110–117.

Jacob, G.C., J.F. Fellers, S. Simunovic, and J.M. Starbuck (2002). Energy Absorption in Polymer Composites for Automotive Crashworthiness. *Journal of Composite Materials* 36.7, pp. 813–850.

Kress, G. and M. Winkler (2010). Corrugated laminate homogenization model. *Composite Structures* 92.3, pp. 795–810.

Lachambre, J., E. Maire, J. Adrien, and D. Choqueuse (2013). In situ observation of syntactic foams under hydrostatic pressure using X-ray tomography. *Acta Materialia* 61.11, pp. 4035–4043.

Li, Y., Z. Lin, A. Jiang, and G. Chen (2003). Use of high strength steel sheet for lightweight and crashworthy car body. *Materials and Design* 24, pp. 177–182.

Manjunath Yadav, S., K.V. Arun, S. Basavarajappa, and S. Kumar (2017). Polymer-Plastics Technology and Engineering Collapse Mechanism of Foam Cored Sandwich Structures Under Compressive Load.

Marek, A. and T. Garbowski (2015). Homogenization of sandwich panels. *Computer Assisted Methods in Engineering and Science*, pp. 39–50.

Marsavina, L., J. Kováčik, and E. Linul (2016). Experimental validation of micromechanical models for brittle aluminium alloy foam. *Theoretical and Applied Fracture Mechanics* 83, pp. 11–18.

Mohr, D. and T. Wierzbicki (2005). On the Crashworthiness of Shear-Rigid Sandwich Structures. *Journal of Applied Mechanics* 73.4, pp. 633–641.

Nayak, S.K., A.K. Singh, A.D. Belegundu, and C.F. Yen (2013). Process for design optimization of honeycomb core sandwich panels for blast load mitigation, pp. 749–763.

Oldenburg, M. and G. Lindkvist (2011). Tool thermal conditions for tailored material properties. *HTM - Haerterei-Technische Mitteilungen* 66.6, pp. 329–334.

Ottosen, N.S. and H. Petersson (1992). *Introduction to the finite element method*. Prentice Hall, p. 410.

Ottosen, N.S. and M. Ristinmaa (2005). *The mechanics of constitutive modeling*. Elsevier, p. 745.

Park, C. and S. Nutt (2000). PM synthesis and properties of steel foams. *Materials Science and Engineering: A* 288.1, pp. 111–118.

Qin, D., T.F. Stocker, G.-k. Plattner, M.M. Tignor, S.K. Allen, J. Boshung, A. Nauels, Y. Xia, V. Bex, and P.M. Midgley (2014). *Climate Change 2013: The Physical Science Basis*. Tech. rep., p. 1535.

Reyes, A., O.S. Hopperstad, T. Berstad, A.G. Hanssen, and M. Langseth (2003). Constitutive modeling of aluminum foam including fracture and statistical variation of density. *European Journal of Mechanics, A/Solids* 22.6, pp. 815–835.

Saber, A.Y., G.K. Venayagamoorthy, and S. Member (2016). Plug-in Vehicles and Renewable Energy Sources for Cost and Emission Reductions Plug-in Vehicles and Renewable Energy Sources for Cost and Emission Reductions. 58.May 2011, pp. 1229–1238.

Schreyer, H.L., R.F. Kulak, and J.M. Kramer (1979). Accurate Numerical Solutions for Elastic - Plastic Models. *Journal of Pressure Vessel Technology* 101.79, pp. 226–234.

Smith, B., S. Szyniszewski, J. Hajjar, B. Schafer, and S. Arwade (2012). Steel foam for structures: A review of applications, manufacturing and material properties. *Journal of Constructional Steel Research* 71, pp. 1–10.

Stevanovic, Aleksandar, Jelka, Zhang, Kai, Batterman, and Stuart (2009). Optimizing Traffic Control to Reduce Fuel Consumption and Vehicular Emissions.

Sulong, M.A., M. Vesenjak, I.V. Belova, G.E. Murch, and T. Fiedler (2014). Compressive properties of Advanced Pore Morphology (APM) foam elements. *Materials Science and Engineering: A* 607, pp. 498–504.

Szyniszewski, S.T., B.H. Smith, J.F. Hajjar, B.W. Schafer, and S.R. Arwade (2014). The mechanical properties and modeling of a sintered hollow sphere steel foam. *Materials and Design* 54, pp. 1083–1094.

Szyniszewski, S., B. Smith, S. Arwade, J. Hajjar, and S. Benjamin (2012). Tensile and shear element erosion in metal foams. *12th International LS-DYNA Users Conference* 1, pp. 1–10.

thyssen-krupp TriBond composite (2018).

Timoshenko, S. (1983). *History of strength of materials : with a brief account of the history of theory of elasticity and theory of structures*. [New ed.] New York: Dover.

Vinson, J.R. (2005). Sandwich Structures: Past, Present and Future. *Sandwich Structures 7: Advancing with Sandwich Structures and Materials: Proceedings of the 7th International Conference on Sandwich Structures*, pp. 3–12.

Weinenborn, O., C. Ebert, and M. Gude (2016). Modelling of the strain rate dependent deformation behaviour of rigid polyurethane foams. *Polymer Testing* 54, pp. 145–149.

Xia, Y., M.I. Friswell, and E.I. Saavedra Flores (2012). Equivalent models of corrugated panels. *International Journal of Solids and Structures* 49, pp. 1453–1462.

Zhang, Y., G. Sun, X. Xu, G. Li, X. Huang, J. Shen, and Q. Li (2013). Identification of material parameters for aluminum foam at high strain rate. *Computational Materials Science* 74, pp. 65–74.

Zhou, X.Q., D.Y. Yu, X.Y. Shao, S. Wang, and Y.H. Tian (2014). Asymptotic analysis on flexural dynamic characteristics for a sandwich plate with periodically perforated viscoelastic damping material core. *Composite Structures* 119, pp. 487–504.

Zhou, X.Q., D.Y. Yu, X.Y. Shao, S. Wang, and S.Q. Zhang (2016). Asymptotic analysis for composite laminated plate with periodically fillers in viscoelastic damping material core. *Composites Part B: Engineering* 96, pp. 45–62.

Zhou, X.Q., D.Y. Yu, X.Y. Shao, S.Q. Zhang, and S. Wang (2016). Research and applications of viscoelastic vibration damping materials: A review. *Composite Structures* 136, pp. 460–480.

Zupan, M., C. Chen, and N.A. Fleck (2003). The plastic collapse and energy absorption capacity of egg-box panels. *International Journal of Mechanical Sciences* 45.5, pp. 851–871.

Appended Papers

Paper A

Homogenization, modeling and evaluation of stiffness for bidirectionally corrugated cores in sandwich panels

Authors:
Samuel Hammarberg, Jörgen Kajberg, Göran Lindkvist, Pär Jonsén

To be submitted.

Homogenization, modeling and evaluation of stiffness for bidirectionally corrugated cores in sandwich panels

Samuel Hammarberg, Jörgen Kajberg, Göran Lindkvist, Pär Jonsén

Abstract

In order to achieve a sustainable society, legislations force the vehicle industry to lower greenhouse gas emissions, such as carbon dioxide and nitrogen oxide. For the vehicle industry to fulfill these demands, new materials and methods are required, for construction of the body in white. Methods for lightweight have been developed during the last decades. In the present work, it is shown that current vehicle components for structural stiffness, are possible to replace with lightweight steel sandwich panels with bidirectionally corrugated cores. Numerical computational time is kept low by introducing a homogenization procedures. It is found that, by introducing these panels, weight is reduced by 60% compared to a solid sheet panel of equivalent stiffness. The homogenization procedure reduces the computational time with up to 99 %. Thus, the suggested panels are promising lightweight contenders for structural stiffness applications.

1 Introduction

Awareness of the importance of creating a sustainable society is an ever increasing area of interest. For a sustainable future all areas of society, from food production to transportation, must be permeated.

Transportation, in itself, receives a lot of attention with respect to sustainability as well as pollution. Regulations of greenhouse gas (GHG) emissions, such as carbon dioxide and nitrogen oxide, contribute to this attention. Ways of reducing such emissions include increasing energy efficiency of current engines, renewable fuel, and lowering weight of vehicle components while maintaining performance such as crashworthiness. A fourth option is of course electrical vehicles where the electricity is generated by renewable energy sources such as solar power and wind power. However, reduced weight of vehicle components is beneficial independent on what propels the vehicle forward.

For a vehicle with a combustion engine a benefit of lighter components is a decreased fuel consumption, leading to less emissions. A lighter heavy duty vehicle, with maintained strength, allows higher payload, reducing the number of trips required for transportation. The electric vehicle would increase its range with lighter components, as well as reduce emissions depending on how the electricity, running the vehicle, is produced.

Methods to reduce weight for body-in-white parts of cars have been under development

during the last decades. One example is press-hardening of boron steels to produce crashworthiness parts, where forming and hardening are performed simultaneously resulting high-strength and great form accuracy at a low cost. By controlling the temperature of the forming tools, either cooler or hotter zones could be obtained and the final properties of the part may therefore be tailor-made with respect to strength and ductility. Hence, a press-hardened part may have both softer as well and harder regions. The weight-saving potential by using high-strength steels is however correlated to thinner gauges. Too thin sections might jeopardize the structural stiffness despite its high-strength. In order to benefit from the high-strength without losing structural stiffness sandwich solutions are attractive. The concept of the sandwich is a lightweight material, or a combination of several, placed between two stiff solid sheets. Proper choice of core material makes it possible to achieve a larger thickness than for a solid core, which results in an improved structural stiffness as long as the core is prevented from collapsing. To hinder collapse, the shear and uniaxial stiffness are of importance. Suitable materials to be used in sandwich cores include foams based on aluminum, steel or polymers. Other possibilities for cores are honeycomb patterns and corrugated plates. A summary of the mentioned cores is given in the following.

In the work performed by Zhang et al., 2013, it is stated that aluminum foams is a common choice for enhancing crashworthiness of vehicles. Their work is dedicated to the characterization of material parameters for aluminum foam at high strain rates. A similar statement is found in Reyes et al., 2003, where aluminum foam is suggested as a proper choice for energy absorption. In in their work, a constitutive model, based on Deshpande and Fleck, 2000, is evaluated by comparison of experiments and simulations of sandwiches with aluminum foam cores.

Studies of steel foam, with respect to characterization and simulation, can be found e.g. in Smith et al., 2012; Mapelli et al., 2013; Szyniszewski et al., 2014; Park and Nutt, 2000. Potential advantages with steel foam, over aluminum foam, are increased strength and specific stiffness, lower material cost, higher melting temperature and better compatibility with steel structure (Park and Nutt, 2000). Furthermore, recycling of a structure solely based on steel requires less energy and is therefore beneficial. A detailed review of steel foam, manufacturing methods, and applications can be found in Smith et al., 2012. Foams based on other bulk materials are also available, such as polymer foams investigated in e.g. Liu and Subhash, 2004; Liu, Subhash, and Gao, 2005; Bartl et al., 2009.

Another weight-saving approach is the use of geometric patterns, such as honeycomb, to to keep the face plates apart for an increased bending stiffness, see Aktay et al., 2008; Nayak et al., 2013. Also, panels with corrugated cores for stiffness applications are found in Biancolini, 2005; Kress and Winkler, 2010; Xia et al., 2012; Bartolozzi et al., 2013; Marek and Garbowski, 2015. Typically, some periodic function describes the geometry of the corrugated plate. Due to the repetetive pattern, each period can be characterized using a unit cell. A variant of this type of core, is a bidirectionally corrugated core utilized, for instance, by Chomphan and Leekitwattana, 2011 to redistribute the stresses within the sandwich panel. A similar type of bidirectionally corrugated core is investigated by

Besse and Mohr, 2012, where a detailed model of a unit cell is created from which shear stiffness is found. Further studies on such cores for energy absorption applications are conducted by Zupan et al., 2003, where it is found that the panel is a competitor if compared to metallic foams considering costs.

In order to introduce lightweight material solutions to, for example, the car industry, it is of great importance that accurate simulation methodologies are available to predict the material response in situations such as forming operation and crash. The simulation methodologies should be time-efficient to facilitate design optimization regarding weight, stiffness and crashworthiness already in the early product development. The complex geometries of the core materials have a drawback when it comes to modelling with the finite element method. For example, the pore size of the foams is in the order of microns, causing impractical number of elements to discretize the exact geometry. It is however reasonably possible to discretize corrugated cores, such as honeycomb, although the number of elements in case the panels are used in a larger structure demand high computation power. The approach to handle this challenge is to describe the combination of the complex core and the face plates with averaging equivalent finite element by so-called homogenization. The number of elements is thereby drastically reduced. Methods for homogenization of corrugated plates are presented inBiancolini, 2005; Kress and Winkler, 2010; Xia et al., 2012; Bartolozzi et al., 2013; Marek and Garbowski, 2015, where both analytic and numeric approaches are presented.

Thus it is found, in the aforementioned works, that corrugated panels are suitable for structural stiffness applications and by adopting homogenization reasonable computational costs are obtained. For corrugated panels a characterization method is found (Bartolozzi et al., 2013), where a detailed model of a unit cell is subjected to a state of shear deformation to predict its shear stiffness.

The present works aims to bring forth lightweight sandwich structures which are able to replace current vehicle components. A further aim is to reduce the numerical computational time for the sandwiches by adopting a homogenization procedure. Two panels, denoted Type A and Type B, with bidirectionally corrugated cores are suggested for stiffness applications. Numerical models of the sandwiches are created and subjected to three-point bending. The response of the sandwich is compared to the response of two references models, consisting of solid steel sheets with equivalent stiffness and weight respectively.

Detailed models with a high amount of elements are required for the numerical discretization of the bidirectionally corrugated cores. In an effort to address this issue, a homogenization procedure is applied to obtain an equivalent core material. The equivalent material is introduced into the sandwich panel through two approaches. In the initial approach solid elements are utilized for representing the equivalent material of the core, while the outer face plates are modeled using shell elements. This approach reduces both the number of elements and the computational time, even though solid elements are utilized. The second approach uses one layer of shell elements to model the entire panel. At each integration point, through the thickness, the corresponding material data is defined. This method further reduces the number of elements and computational time.

In order to validate the numerical models, a sandwich panel with a Type A core has been manufactured. The panel is subjected to an experimental three point bend and the obtained response is compared and evaluated against the numerical data.

2 Geometries and materials

In the present work sandwiches with bidirectionally corrugated cores are suggested for stiffness applications. The panels are based on 0.4 millimeters thick boron steel, 22MnB5, for both face plates and core. Young's modulus and Poisson's ratio is given as 206 GPa and 0.3 respectively, with a density of 7850 kg/m^3. The bidirectional geometry of the core is obtained through cold-rolling using patterned rolls. The envelope surfaces of the rolls are are derived from a given sinusoidal function, thus giving the core its desired geometry. The panel, denoted Type A, is presented in Figure 1. Joining between face plates and core is performed by laser welding. Due to springback, the manufactured cores deviate slightly from the sinusoidal pattern of the rolls. Thus, the wavelength and the amplitude must be altered when creating the numerical model. This is done by measuring both wavelength, λ and peak to peak amplitude, A, of the manufactured panels, which are found to be 139/9 millimeters per period and 2.9 millimeters respectively. A total of 32 and 4 periods are found in the x- and y-direction respectively. Thus the length and width of the panel is approximated to 32λ and 4λ respectively. For the numerical simulations a CAD version of the geometry is created. This is presented in Figure 2. To increase the welding area for an improved bond, an alternative core geometry, Type B, is suggested where the peaks are flattened, see Figure 3

For the homogenization process, the core is characterized with respect to its elastic properties. For the given core geometries a repeating pattern of the core is identified, namely a unit cell, which is used for the characterization and homogenization processes. The unit cells are presented in Figures 4 and 5.

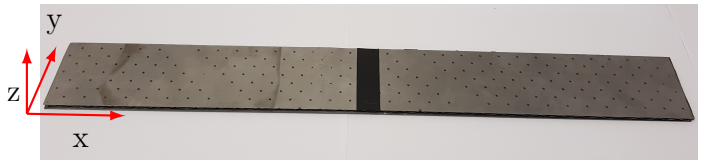

(a) Sandwich panel.

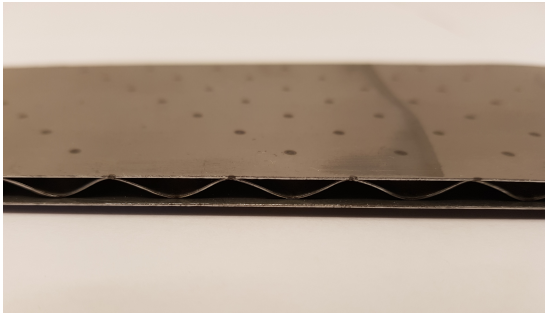

(b) Sandwich panel zoomed in.

Figure 1: Sandwich panel subjected to three point bending for stiffness evaluation.

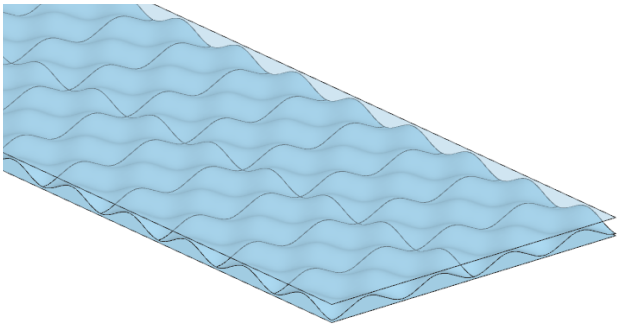

Figure 2: Illustration of the geometry used for numerical simulations of panels with the Type A core.

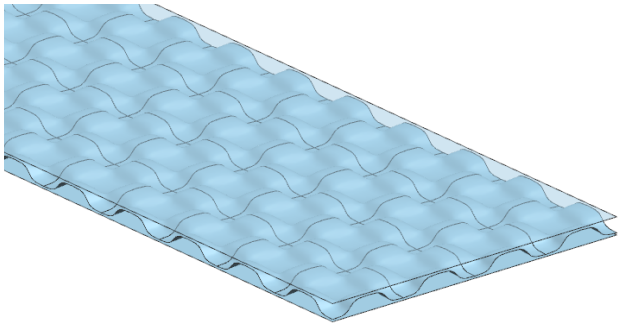

Figure 3: Illustration of the geometry used for numerical simulations of panels with the Type B core.

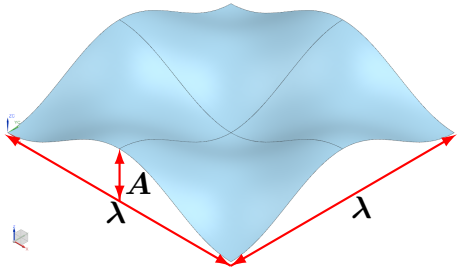

Figure 4: A unit cell used for identification of stiffness properties for the Type A core. The value of λ is set to 139/9 millimeters, corresponding to the wavelength of the function. A is the peak to peak amplitude and has a value of 2.9 millimeters.

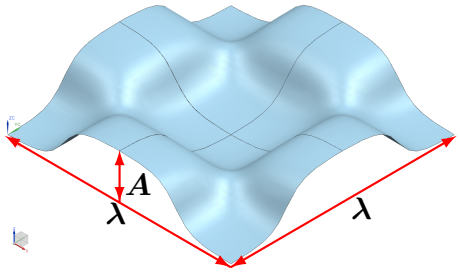

Figure 5: A unit cell used for identification of stiffness properties for the Type B core. The value of λ is set to 139/9 millimeters, corresponding to the wavelength of the function. A is the peak to peak amplitude and has a value of 2.9 millimeters.

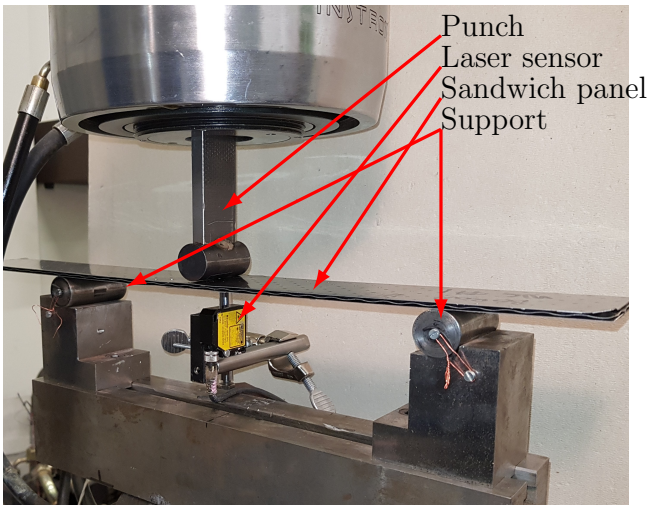

Figure 6: Experimental setup for three point bending of a sandwich panel.

3 Experiments

In order to find the stiffness of the sandwich panel with a bidirectionally corrugated core, see Figure 1, three-point-bending is performed. The experimental setup, presented in Figure 6, is carried out using a servo-hydraulic testing machine, Instron 1272. The applied force is measured by the load of the testing machine. The load line displacement is tracked by a laser sensor, measuring the deflection of the panel. Three specimens of the panel are tested and compared to see how consistent the response from the panels are. Distance between the supports is set to 300 millimeters. The diameters of the supporting rolls and punch are 25 millimeters.

4 Laminate theory

One of the modeling approaches, for the homogenized panels, adopts one layer of shell elements to represent the panel. Laminate shell theory is utilized for predicting stiffness in a proper manner. Thus, an introduction to the classical laminate shell theory in the given in the current section.

In general a laminate consists of two or more laminae. The laminae are bonded together to generate a structural element. Typically, the layers of the laminate, the laminae, are oriented in such a manner that the laminate can withstand loading in several directions. In the following, derivation of stiffness and strength of such material is presented. For the classical laminate theory, the aim is to find accurate simplifying assumptions that reduce the problem from three dimensions to two dimensions (such as plane stress condition).

The plane stress-strain relationship for a laminae of an orthotropic material given in

the principal material coordinates is written as

$$\begin{bmatrix} \sigma_1 \\ \sigma_2 \\ \tau_{12} \end{bmatrix} = \begin{bmatrix} Q_{11} & Q_{12} & 0 \\ Q_{21} & Q_{22} & 0 \\ 0 & 0 & Q_{66} \end{bmatrix} \begin{bmatrix} \epsilon_1 \\ \epsilon_2 \\ \gamma_{12} \end{bmatrix} \tag{1}$$

where

$$Q_{11} == \frac{S_{22}}{S_{11}S_{22} - S_{12}^2} \tag{2}$$

$$Q_{12} = -\frac{S_{12}}{S_{11}S_{22} - S_{12}^2} \tag{3}$$

$$Q_{22} = \frac{S_{11}}{S_{11}S_{22} - S_{12}^2} \tag{4}$$

$$Q_{66} = \frac{1}{S_{66}} \tag{5}$$

and

$$S_{11} = \frac{1}{E_1} \tag{6}$$

$$S_{12} = -\frac{\nu_{12}}{E_1} = -\frac{\nu_{21}}{E_2} \tag{7}$$

$$S_{22} = \frac{1}{E_2} \tag{8}$$

$$S_{66} = \frac{1}{G_{12}}. \tag{9}$$

It should be noted that E_i and G_{12} are material data for the particular laminae. Furthermore, note that Equation (1) is only valid for the principal material directions. For any other in-plane coordinate system the following holds true

$$\begin{bmatrix} \sigma_x \\ \sigma_y \\ \tau_{xy} \end{bmatrix} = \begin{bmatrix} Q'_{11} & Q'_{12} & Q'_{16} \\ Q'_{21} & Q'_{22} & Q'_{26} \\ Q'_{16} & Q'_{26} & Q'_{66} \end{bmatrix} \begin{bmatrix} \epsilon_x \\ \epsilon_y \\ \gamma_{xy} \end{bmatrix}. \tag{10}$$

The transformed stiffness matrix, Q'_{ij}, is given by the following, in accordance with Figure 7

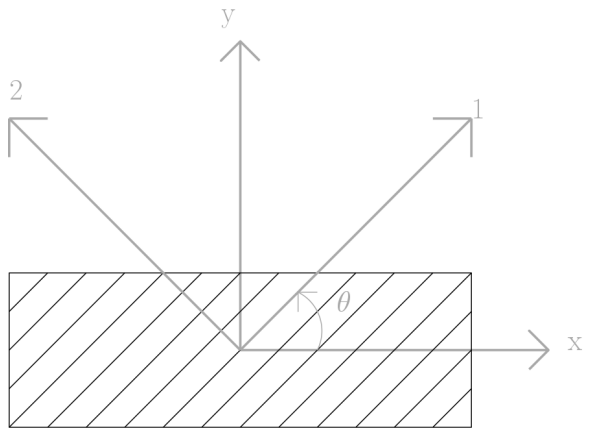

Figure 7: Illustration of a laminae. The fiber direction is aligned with the 1-direction, rotated θ counterclockwise from the x-direction.

$$\begin{aligned}
Q'_{11} &= Q_{11} \cdot cos^4\theta + 2(Q_{12} + 2Q_{66})sin^2\theta cos^2\theta + Q_{22}sin^4\theta \\
Q'_{12} &= (Q_{11} + Q_{22} - 4Q_{66})\, sin^2\theta cos^2\theta + Q_{12}\,(sin^4\theta + cos^4\theta) \\
Q'_{22} &= Q_{11} \cdot sin^4\theta + 2(Q_{12} + 2Q_{66})sin^2\theta cos^2\theta + Q_{22}cos^4\theta \\
Q'_{16} &= (Q_{11} - Q_{12} - 2Q_{66})\, sin\theta cos^3\theta + (Q_{12} - Q_{22} + 2Q_{66})sin^3\theta cos\theta \\
Q'_{26} &= (Q_{11} - Q_{12} - 2Q_{66})\, sin^3\theta cos\theta + (Q_{12} - Q_{22} + 2Q_{66})sin\theta cos^3\theta \\
Q'_{66} &= (Q_{11} + Q_{22} - 2Q_{12} - 2Q_{66})\, sin^2\theta cos^2\theta + Q_{66}(sin^4\theta + cos^4\theta)
\end{aligned} \tag{11}$$

Equation (1) and Equation (10) represent the stress strain relationship in a lamina in the principal and the general direction respectively. Then, for a given layer of a laminate, say the k^{th} layer, the following is established

$$[\sigma]_k = [Q']_k\,[\epsilon]_k\,. \tag{12}$$

In the theory of classical laminates it is assumed that the laminae are perfectly bonded. The displacements are continuous across lamina boundaries and no shear deformation occurs in the bond. These assumptions lead to the assumption that the laminate acts as a single plate or shell. Furthermore, the laminate is assumed to be thin and shearing strains in planes perpendicular to the middle surface are equal to zero. These assumptions for one lamina are equal to the Kirchhoff hypothesis for plates, so the strains, derived using the deformation of Figure 8, can be written as

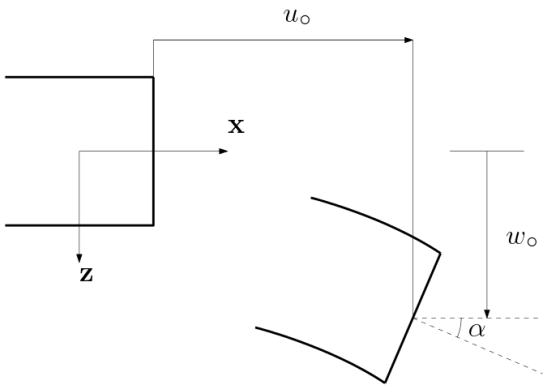

Figure 8: Illustration of deformations in the x-z plane used for deriving strain relationships based on the Kirchhoff hypothesis.

$$\epsilon_x = \frac{\partial u}{\partial x} \tag{13}$$

$$\epsilon_y = \frac{\partial v}{\partial y} \tag{14}$$

$$\gamma_{xy} = \frac{\partial u}{\partial y} + \frac{\partial v}{\partial x} \tag{15}$$

where the displacement u, derived from Figure 8 at any point through the thickness of the laminate and the angle, α, are obtained as

$$u = u_\circ - \frac{\partial w_\circ}{\partial x}. \tag{16}$$

$$\alpha = \frac{\partial w_\circ}{\partial x} \tag{17}$$

The displacement in the y-direction, out of the plane of Figure 8, is obtained in a similar manner

$$v = v_\circ - z\frac{\partial w_\circ}{\partial y}. \tag{18}$$

Inserting the displacements of Equations (16) and (18) into the expressions for the strains in Equations (13), (14), and (15) the following expressions are obtained

$$\epsilon_x = \frac{\partial u_\circ}{\partial x} - z\frac{\partial^2 w_\circ}{\partial x^2} \tag{19}$$

$$\epsilon_y = \frac{\partial v_\circ}{\partial y} - z\frac{\partial^2 w_\circ}{\partial y^2} \tag{20}$$

$$\gamma_{xy} = \frac{\partial u_\circ}{\partial y} + \frac{\partial v_\circ}{\partial x} - 2z\frac{\partial^2 w_\circ}{\partial x \partial y} \tag{21}$$

which can be written as

$$\begin{bmatrix} \epsilon_x \\ \epsilon_y \\ \gamma_{xy} \end{bmatrix} = \begin{bmatrix} \epsilon_x^\circ \\ \epsilon_y^\circ \\ \gamma_{xy}^\circ \end{bmatrix} + z \begin{bmatrix} \kappa_x \\ \kappa_y \\ \kappa_{xy} \end{bmatrix} \tag{22}$$

where ϵ_x°, ϵ_y° and γ_{xy}° correspond to the middle surface strains, and κ_x, κ_y and κ_{xy} correspond to the middles surface curvature according to

$$\begin{bmatrix} \epsilon_x^\circ \\ \epsilon_y^\circ \\ \gamma_{xy}^\circ \end{bmatrix} = \begin{bmatrix} \frac{\partial u_\circ}{\partial x} \\ \frac{\partial v_\circ}{\partial y} \\ \frac{\partial u_\circ}{\partial y} + \frac{\partial v_\circ}{\partial x} \end{bmatrix} \tag{23}$$

$$\begin{bmatrix} \kappa_x \\ \kappa_y \\ \kappa_{xy} \end{bmatrix} = - \begin{bmatrix} \frac{\partial^2 w_\circ}{\partial x^2} \\ \frac{\partial^2 w_\circ}{\partial y^2} \\ 2\frac{\partial^2 w_\circ}{\partial x \partial y} \end{bmatrix}. \tag{24}$$

Inserting Equation (22) into Equation (12) the following expression for the stress of the k^{th} layer is obtained

$$\begin{bmatrix} \sigma_x \\ \sigma_y \\ \tau_{xy} \end{bmatrix} = \begin{bmatrix} Q'_{11} & Q'_{12} & Q'_{16} \\ Q'_{21} & Q'_{22} & Q'_{26} \\ Q'_{16} & Q'_{26} & Q_{66} \end{bmatrix} \left[\begin{bmatrix} \epsilon_x^\circ \\ \epsilon_y^\circ \\ \gamma_{xy}^\circ \end{bmatrix} + z \begin{bmatrix} \kappa_x \\ \kappa_y \\ \kappa_{xy} \end{bmatrix} \right]. \tag{25}$$

Integrating Equation (25) over the thickness results in the resultant forces and moments acting on the laminae, which is given by

$$\begin{bmatrix} N_x \\ N_y \\ N_{xy} \end{bmatrix} = \int_{-t/2}^{t/2} \begin{bmatrix} \sigma_x \\ \sigma_y \\ \tau_{xy} \end{bmatrix} dz = \sum_{k=1}^{N} \int_{z_{k-1}}^{z^k} \begin{bmatrix} \sigma_x \\ \sigma_y \\ \tau_{xy} \end{bmatrix} dz \tag{26}$$

$$\begin{bmatrix} N_x \\ N_y \\ N_{xy} \end{bmatrix} = \int_{-t/2}^{t/2} \begin{bmatrix} \sigma_x \\ \sigma_y \\ \tau_{xy} \end{bmatrix} z dz = \sum_{k=1}^{N} \int_{z_{k-1}}^{z^k} \begin{bmatrix} \sigma_x \\ \sigma_y \\ \tau_{xy} \end{bmatrix} z dz \tag{27}$$

which are both rearranged on the following form

$$\begin{bmatrix} N_x \\ N_y \\ N_{xy} \end{bmatrix} = \sum_{k=1}^{N} \begin{bmatrix} Q'_{11} & Q'_{12} & Q'_{16} \\ Q'_{21} & Q'_{22} & Q'_{26} \\ Q'_{16} & Q'_{26} & Q'_{66} \end{bmatrix} \left[\int_{z_{k-1}}^{z:k} \begin{bmatrix} \epsilon_x^\circ \\ \epsilon_y^\circ \\ \gamma_{xy}^\circ \end{bmatrix} dz + \int_{z_{k-1}}^{z_k} \begin{bmatrix} \kappa_x \\ \kappa_y \\ \kappa_{xy} \end{bmatrix} z dz \right] \tag{28}$$

$$\begin{bmatrix} M_x \\ M_y \\ M_{xy} \end{bmatrix} = \sum_{k=1}^{N} \begin{bmatrix} Q'_{11} & Q'_{12} & Q'_{16} \\ Q'_{21} & Q'_{22} & Q'_{26} \\ Q'_{16} & Q'_{26} & Q'_{66} \end{bmatrix} \left[\int_{z_{k-1}}^{z:k} \begin{bmatrix} \epsilon_x^\circ \\ \epsilon_y^\circ \\ \gamma_{xy}^\circ \end{bmatrix} z dz + \int_{z_{k-1}}^{z_k} \begin{bmatrix} \kappa_x \\ \kappa_y \\ \kappa_{xy} \end{bmatrix} z^2 dz \right] \tag{29}$$

A further simplification can be achieved by introducing the following

$$A_{ij} = \sum_{k=1}^{N} (Q'_{ij})_k (z_k - z_{k-1}) \tag{30}$$

$$B_{ij} = \frac{1}{2} \sum_{k=1}^{N} (Q'_{ij})_k (z_k^2 - z_{k-1}^2) \tag{31}$$

$$D_{ij} = \frac{1}{3} \sum_{k=1}^{N} (Q'_{ij})_k (z_k^3 - z_{k-1}^3) \tag{32}$$

Equation (28) and (29) can then be written as

$$\begin{bmatrix} N_x \\ N_y \\ N_{xy} \end{bmatrix} = \begin{bmatrix} A_{11} & A_{12} & A_{16} \\ A_{12} & A_{22} & A_{26} \\ A_{16} & A_{26} & A_{66} \end{bmatrix} \begin{bmatrix} \epsilon_x^\circ \\ \epsilon_y^\circ \\ \gamma_{xy}^\circ \end{bmatrix} + \begin{bmatrix} B_{11} & B_{12} & B_{16} \\ B_{12} & B_{22} & B_{26} \\ B_{16} & B_{26} & B_{66} \end{bmatrix} \begin{bmatrix} \kappa_x \\ \kappa_y \\ \kappa_{xy} \end{bmatrix} \tag{33}$$

$$\begin{bmatrix} M_x \\ M_y \\ M_{xy} \end{bmatrix} = \begin{bmatrix} A_{11} & A_{12} & A_{16} \\ A_{12} & A_{22} & A_{26} \\ A_{16} & A_{26} & A_{66} \end{bmatrix} \begin{bmatrix} \epsilon_x^\circ \\ \epsilon_y^\circ \\ \gamma_{xy}^\circ \end{bmatrix} + \begin{bmatrix} D_{11} & D_{12} & D_{16} \\ D_{12} & D_{22} & D_{26} \\ D_{16} & D_{26} & D_{66} \end{bmatrix} \begin{bmatrix} \kappa_x \\ \kappa_y \\ \kappa_{xy} \end{bmatrix} \tag{34}$$

in which A_{ij} corresponds to extensional stiffness, B_{ij} to the bending extension coupling stiffness, and D_{ij} to the bending stiffness. It should be noted that the strain displacement relationship used in derivation of the connection between strains and forces/moments given above holds true for plates. In the case of shells a more complicated strain-displacement relationship may be necessary.

5 Homogenization

In the current section a detailed presentation is given of the homogenization procedure adopted in the present work. This includes the models used for representing the volume element, as well as how the fundamental constants, governing the elastic behavior, are determined.

5.1 Work procedure

The aim of the homogenization process is to determine the fundamental constants, presented in Table 1, governing the elastic behavior of the sandwich cores of Figures 2 and 3. When the constants are determined they are imposed on an equivalent material. The equivalent material is homogeneous, with the same outer dimensions as the core of the sandwiches. It also requires less finite elements for discretization which reduces the computational time. This makes numerical simulations of the panels in Figure 2 and Figure 3 less time consuming, being the aim of the homogenization procedure.

Table 1: Elastic properties to be determined in general for an orthotropic material. The x-coordinate corresponds to the longitudinal direction, the y-coordinate corresponds to the width, and the z-coordinate is normal to the panel.

Young's Modulus	Shear Modulus	Poisson's ration
E_{xx}	G_{xz}	ν_{xy}
E_{yy}	G_{yx}	ν_{yz}
E_{zz}	G_{zy}	ν_{zx}

Table 2: Reduced number of unique elastic properties to be determined for the unit cells.

Young's Modulus	Shear Modulus	Poisson's ration
$E_{xx} = E_{yy}$	$G_{xz} = G_{zy}$	ν_{yx}
E_{zz}	G_{xy}	$\nu_{zx} = \nu_{yz}$

As a first step of the homogenization procedure a unit cell, representing the geometry of the core, is identified, see Figure 4 and Figure 5. For each unit cell nine elastic constants of Table 1 must be determined. These constants are found by subjecting the unit cells to the appropriate state of deformation, from which these nine constants are found. In general, three states of deformation are required for determining the three values of Young's moduli and Poisson's ratios, as well as three for determining the shear moduli. For the current case, the unit cells posses in-plane symmetry and it is evident that $E_{xx} = E_{yy}$, $G_{zx} = G_{zy}$ and $\nu_{xz} = \nu_{yz}$. Thus the unique number of constants to be determined are reduced from nine to six, see Table 2.

The obtained values of Young's moduli and the shear moduli are given to the equivalent material, so when the equivalent material is loaded uniaxially in the x-direction its stiffness corresponds to that of the unit cell of Type A or Type B. Likewise, if the equivalent material is loaded in pure shear it should produce the corresponding stiffness of the unit cells.

In order to impose the states of deformation on the unit cells a numerical method is adopted. The method is similar to of Bartolozzi et al., 2013, where FEA is utilized to impose the proper deformation. From the results of the FEA the stress and strain required to deform the unit cells are obtained, and for each deformation state the corresponding elastic constants are obtained. In Section 5.2 this is presented in more detail.

With the constants determined, it is possible to reduce the complexity of the core geometry by imposing the elastic properties on an equivalent model of the core. An illustration of the reduced complexity is presented in Figure 9 where both the complex core and the equivalent model are presented. The outer dimension of the core are kept constant, and the homogenized model should have a reduced number of elements for the homogenization process to meaningful, while still being able to predict the structural stiffness.

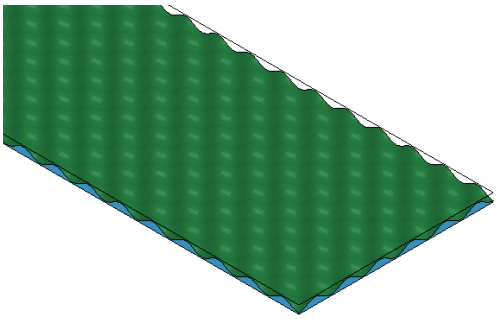

(a) Type A core.

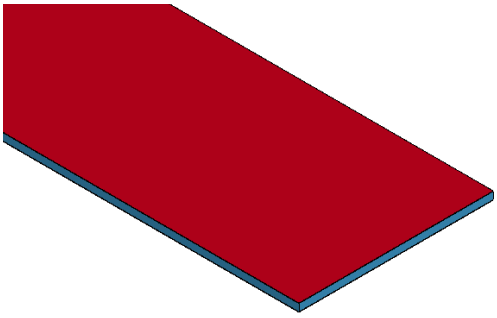

(b) Equivalent core.

Figure 9: Illustrating going from a detailed core to a homogenized equivalent core with equal outer dimensions.

5.2 Modeling of unit cells

A numerical approach is adopted for determining the elastic properties of the unit cells presented in Figures 4 and 5. The multi-physics solver LS-DYNA is adopted with its implicit solution scheme triggered. Initially, fully integrated shell elements (element formulation 16 within LS-DYNA) with a size of 1 mm are used to represent the geometry of the unit cell. However, as can be seen in Figure 10b a shell mesh size of 1 mm does not quite capture the curvature of the unit cell. Reducing the size of the shell element results in a poor aspect ratio. Therefor, a convergence study utilizing fully integrated solid elements (ELFORM = 2 within LS-DYNA) is performed for each elastic constant. It should be noted that for the convergence study only cubic solid elements (all side lengths set equal) are utilized. The amount of solid elements through the thickness of the plate is incrementally increased until the stiffness response converged. Convergence is assumed when the following condition is fulfilled

$$Convergence = \frac{\xi_i - \xi_{i+1}}{\xi_i} \leq 1\% \tag{35}$$

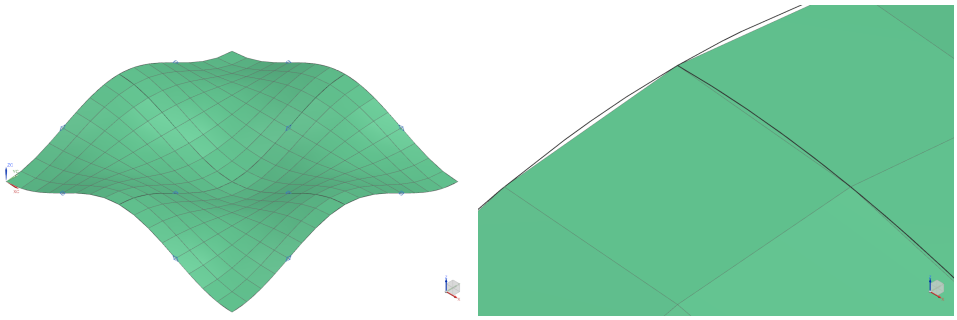

(a) Isometric view. (b) Isometric view zoomed in.

Figure 10: Unit cell of Type A with a shell mesh of 1 mm. It is illustrated how a shell mesh of 1 mm not quite captures the curvature of the unit cell.

where ξ_i corresponds to the stiffness response for i solid elements through the thickness. The obtained results are compared to the results obtained using shell elements.

5.3 Determination of elastic constants

In the current section, a detailed description is given on finding the elastic properties of an arbitrary unit cell. A numerical approach is adopted where FEA is used to displace the unit cell in a proper manner to obtain the constants of interest. Two cores are investigated and their corresponding unit cells are presented in Figure 4 and Figure 5.

Due to the shape of the Type A core it is not possible to capture the curvature of the geometry while maintaining a proper aspect ratio of the shell elements. Instead, cubical solid elements with selective reduced integration are adopted. A choice which allows for a proper representation of geometry and at the same preventing hourglassing. Generally, five solid elements through the thickness are used.

Equivalent Young's moduli E_x and E_y

Determination of Young's moduli is performed by constraining the nodes on the left hand side of Figure 11 in the x-direction (all other degrees of freedom are unconstrained) while the nodes on the right hand side are given a prescribed displacement. It should be noted that the unit cell has similar side lengths. When the simulation terminates, the sum of the force required to deform the unit cell is found together with the final displacement of the nodes.

For the current case an equivalent area, of the unit cell, perpendicular to the x-direction is calculated as

$$A_{equivalent} = H \cdot L \tag{36}$$

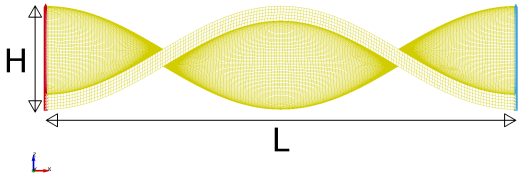

Figure 11: Side view of a unit cell of the Type A core. The marked nodes on the left hand side are constrained in the x-direction whereas the nodes on the right hand side are displaced in the x-direction.

and from the sum of the forces, F acting on the nodes the stress was calculated as

$$\sigma_{xx} = \frac{F}{A_{equivalent}} = \frac{F}{H \cdot L}. \tag{37}$$

From the total displacement, Δ_{xx}, of the unit cell in the x-direction the strain is obtained as

$$\epsilon_{xx} = \frac{\Delta_{xx}}{L}. \tag{38}$$

With stress and strain known in the x-direction the equivalent Young's modulus is determined using Hooke's law:

$$E_{xx} = \frac{\sigma_{xx}}{\epsilon_{xx}} = \frac{F}{H \cdot L} \Big/ \frac{\Delta_{xx}}{L} = \frac{F}{\Delta_{xx} L}. \tag{39}$$

Due to the symmetry planes, the xz-plane and the yz-plane, the equivalent Young's modulus in the y-direction is equivalent to the one in the x-direction.

Equivalent Young's module E_z

In order to determine Young's modulus in the normal direction of the unit cell, the bottom nodes in the four corners are constrained in the z-direction. The nodes on the top, where the amplitude of the greatest, is given a prescribed motion in the negative (compression) z-direction. At termination the force on the nodes, which are given a prescribed displacement, is summed up. With the force and displacement known, Young's modulus in the z-direction is determined. The equivalent area is obtained as

$$A_{equivalent} = L^2 \tag{40}$$

and thus the stress in the negative z-direction is obtained as

$$\sigma_{zz} = \frac{F}{A_{equivalent}} = \frac{F}{L^2} \tag{41}$$

From the total displacement, Δ_{zz}, of the unit cell the strain is obtained as

$$\epsilon_{zz} = \frac{\Delta_{zz}}{H} \tag{42}$$

Applying Hooke's law, Young's modulus is obtained as

$$E_{zz} = \frac{\sigma_{zz}}{\epsilon_{zz}} = \frac{F}{L^2} \Big/ \frac{\Delta_{zz}}{H} = \frac{F \cdot H}{\Delta_{zz} \cdot L^2} \tag{43}$$

Equivalent shear moduli G_{zx} and G_{zy}

To determine the out of the plane shear properties the unit cell of Figure 12 was subjected to shear deformation. The specific stress state is achieved by constraining the corner nodes, which are highlighted in red, in all directions, while subjecting the top nodes to a prescribed displacement. Thus achieving what would be a state of pure shear stress for the equivalent material. From the known displacements and the force requiring to obtain the state of stress, the shear modulus is determined in the following manner. The equivalent area, on which the shear force is acting is given by

$$A_{equivalent} = L^2 \tag{44}$$

and so the stress is obtained as

$$\tau_{zx} = \frac{F_{zx}}{A_{equivalent}} = \frac{F_{zx}}{L^2}. \tag{45}$$

The shear strain is calculated as

$$\gamma_{zx} = \frac{\Delta_{xx}}{H} \tag{46}$$

and according to Hooke's law the following expression for the shear modulus is obtained

$$G_{zx} = \frac{\tau_{zx}}{\gamma_{zx}} = \frac{F_{zx}}{L^2} \frac{\Delta_{xx}}{H} \tag{47}$$

Equivalent shear modulus G_{xy}

In order to determine the in plane shear modulus, the highlighted nodes, in blue, of Figure 13 are given a constrain and the nodes on the opposite side are displaced, both in the y-direction. From the known force and displacement, the shear modulus is determined. The equivalent area on which the force acted is given by

$$A_{equivalen} = H \cdot L \tag{48}$$

and so the shear stress is obtained as

$$\tau_{xy} = \frac{F_{xy}}{A_{equivalent}} = \frac{F_{xy}}{H \cdot L}. \tag{49}$$

The shear strain is given by the following

$$\gamma_{xy} = \frac{\Delta_{yy}}{L} \tag{50}$$

Applying Hooke's law the following expression is obtained for the equivalent, in-plane, shear modulus

$$G_{xy} = \frac{\tau_{xy}}{\gamma_{xy}} = \frac{F_{xy}}{H \cdot L} / \frac{\Delta_{yy}}{L} = \frac{F_{xy}}{H \cdot \Delta_{yy}} \tag{51}$$

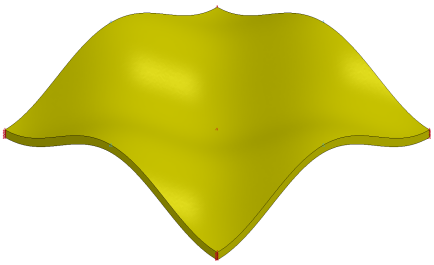

Figure 12: A unit cell of the Type A core, where the nodes associated with the constraints related to out of the plane shearing are highlighted.

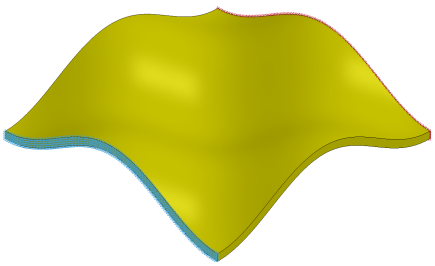

Figure 13: A unit cell of the Type A core, where the nodes associated with the constrains related to the in plane shearing are highlighted.

6 Numerical validation - three-point bending

In the current section the method adopted for verification of the homogenization procedure is presented. The validation is carried out by subjecting sandwich plates to three-

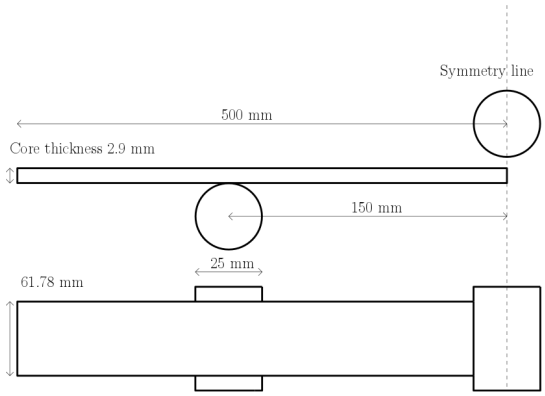

Figure 14: An illustration of the geometry used for the three point bend simulation for validation of stiffness.

point-bending. In Figure 14 the dimensions of the model are presented, and it should be noted that a symmetry condition is applied. Results are compared to experimentally obtained data. Four numerical modeling approaches are adopted. These are listed below.

- Approach #1: Reference model. Shell elements are utilized for both face plates and the core.

- Approach #2: Reference model. Solid elements are utilized for both the face plates and the core.

- Approach #3: Homogenized model where the core is replaced by an equivalent material. The properties found from the homogenization process is applied to the equivalent material by the use of a composite constitutive routine within LS-DYNA. The core is modeled using solid elements and the face plates are modeled using shell elements.

- Approach #4: Homogenized model where the entire panel is modeled using one layer of shell elements. The core is replaced by an equivalent material by using a composite constitutive routine available within LS-DYNA with the material properties obtained from the homogenization procedure. The material through the thickness of the panel is defined at each integration point by utilizing the *PART_COMPOSITE keyword.

A more comprehensive description of the four modeling approaches is given in the following sections. It should be noted that the modeling approach presented below applies to both the Type A and the Type B sandwich cores.

6.1 Approach #1: Reference model - shell elements

This is the reference model where the entire complex core geometry of the sandwich panel is modeled. A total of five parts make up the model: punch, support, upper face plate, core, and lower face plate. This is presented in Figure 15 where a symmetry condition is applied to reduce the number of elements of the model. The discretization is performed using fully integrated shell elements (ELFORM = 16 within LS-DYNA) with a mesh size of 1 millimeter and a thickness of 0.4 mm for all parts. The choice of shell elements may seem contradictory since they to do not quite capture the curvature of the core, as is mentioned in Section 5.2. However, from the results it will be clear that for a three-point bending the discretization is good enough. Five points of integration are used through the thickness. The core and the faceplates consist of hardened boron steel which is modeled using the same constitutive routine and parameters as for the unit cells presented in Section 5.2. The support and the punch are modeled as rigid bodies.

Contacts in the model are handled using a segment based automatic single surface contact. The face plates are spotwelded to the core of the sandwich panel. In the model the spotwelds are represented using beam elements together with the constitutive model *MAT_SPOTWELD as well as the *CONTACT_SPOTWELD keyword. These spotwelds are placed at each maximum and minimum amplitude of the core. For the constitutive model of the spotwelds the same material input data is used as for the hardened boron steel, which is presented in Section 6.2. A displacement of 3 millimeters is given to the punch.

6.2 Approach #2: Reference model - solid Elements

The reference model based on solid elements is equal to the reference model based on shell elements except for the type of elements used. Instead of shell elements, fully integrated solid elements with selectively reduced integration are adopted. For the sandwich (face plates and core) three cubic elements through thickness are used. The support and punch are modeled as rigid bodies.

6.3 Approach #3: Homogenized plate - solid and shell elements

A total of five parts make up the model, where three are associated with the plate and the remaining two correspond to the punch and support. Discretization of the core is performed using fully integrated solid elements (ELFROM = 2 within LS-DYNA). The number of elements in the three orthogonal directions (thickness, width, and length) is varied to find which mesh density is required for the response to be mesh independent, while keeping the computational costs low. In case the dimensions of the solid elements in the XY-plane are much greater than in the z-direction, poor aspect ratios are obtained, and ELFORM = -1 and ELFORM = -2 is used within LS-DYNA. These formulations are intended for solid elements with a poor aspect ratio. Fully integrated shell elements (ELFORM = 16 within LS-DYNA) are used for the face plates (as well as for the support and barrier), with five integration points through the thickness.

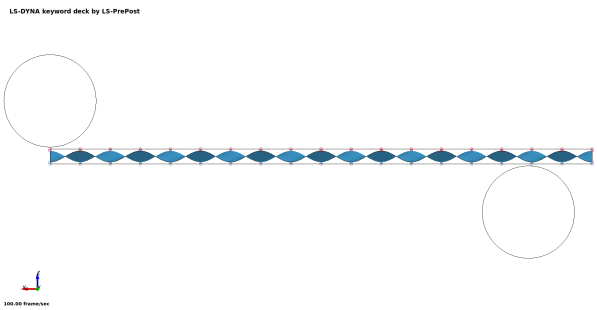

(a) Side view.

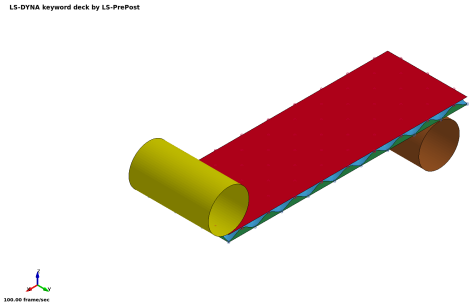

(b) Isometric view.

Figure 15: An illustration of the reference model with a core based on shell elements.

A composite failure model, namely *MAT_059 intended for solid elements within LS-DYNA, is used for modeling of the constitutive behavior of the core. The determined elastic constants are used as input data. The face plates are modeled using the same constitutive routine as for the unit cells of Section 5.2. Punch and supports are modeled as rigid bodies.

A segment based single surface contact algorithm is adopted for handling contacts. As for the reference model the spotwelds between core and face plates are modeled using a spotweld contact algorithm, where the constitutive behavior of the welds is represented using *MAT_100, intended for spotwelds. See Section 6.2 for further information.

6.4 Approach #4: Homogenized plate - part composite

The model consists of three parts: plate, support, and barrier. The plate was modeled using *PART_COMPOSITE within LS-DYNA, see Figure 16. The figure illustrates how each integration point, given by the user, is associated with a thickness and a material identification number. Summation of the thickness of each individual integration point corresponds to the total thickness of the sandwich. For a case where the stiffness varies throughout the thickness of the sandwich, it is recommended to trigger laminate shell

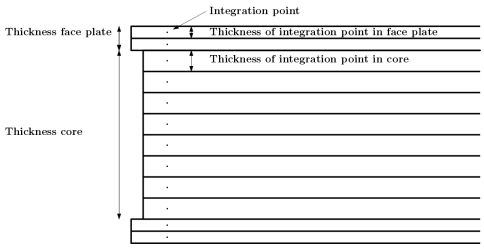

Figure 16: Illustration of how the *PART_COMPOSITE keyword within LS-DYNA is defined in the simulation. Each integration point, defined by the user, is given a thickness and material identification number. The sum of the thickness corresponds to the total thickness of the part.

theory within LS-DYNA, which is done in the *CONTROL_SHELL keyword.

The constitutive routine, *MAT_022, was applied for modeling the core of the sandwich. Young's modulus, shear modulus, and Poisson's ratio are given as input data, for the corresponding directions, as well as density. The face plates are modeled using the constitutive routine as for the unit cells of Section 5.2. The barrier and the support are modeled as rigid bodies.

For handling of the contacts, a segment based single surface contact algorithm is applied. In accordance with classical laminate plate theory, perfect bonding is assumed. Hence, delamination is not included in the mode.

7 Results and discussion

In the current section results are presented and discussed. Initially, results from the homogenization procedure of the Type A and Type B core are presented and discussed. The discussion concerns the modeling approach which is adopted and also how the results converged. This is followed by results and discussion concerning the numerical three-point bending. The results obtained from the numerical models are validated and compared to the experimentally obtained data.

7.1 Homogenization procedure - Type A

The obtained elastic constants for the unit cell of the Type A core are presented in Table 3. As mentioned in Section 5.2, shell elements with proper aspect ratios did not represent the curvature of the core in a satisfactory manner. Therefore, fully integrated solid elements are introduced. It should be noted that in the general case, such elements can produce a too stiff response, as stated in Erhart, 2011. This problem is solved by increasing the number of solid elements through the thickness, or by introducing one of the following element formulations available within LS-DYNA: ELFORM = -1 och ELFORM = -2, with a higher convergence rate for mesh independence. For the homogenization

Table 3: Elastic constants obtained from the unit cell of the Type A core. For the shell elements a mesh size of 1 mm was used, and for the solids 9 cubic elements through the thickness was utlized.

	E_x [GPa]	E_z [GPa]	G_{xy}[GPa]	G_{xz}[GPa]	ν_{xy}	ν_{zx}
Shells	11.27	0.043	1.15	0.79		
Solids	11.08	0.038	1.07	0.4		
Difference	4.35%	13.16%	7.48%	97%		

process, the numbers of solid elements through the thickness are increased until mesh independence was achieved. It was found that the shell elements produced only a slightly stiffer response, except for shear stiffness in the x-z-plane, where the shell elements were almost twice as stiff. This may originate from the shell elements not being able to capture the curvature of the unit cell.

7.2 Three-point bending - Type A

To validate the numerical models of Type A, three manufactured panels (Panel 01, Panel 02 and Panel 03), are subjected to three-point bending. The experimentally obtained results are presented in Figure 17. In the figure it is noted that the stiffness differs somewhat between the three panels. This difference may result from imperfections in the geometry. It is also observed that the face plates were not perfectly plane which may be a result of the laser welding that is carried out to join the face plates to the core.

In Figure 18 the reference model is compared to the experimental data of Panel 01, showing a slight difference in stiffness. This difference in stiffness may arise from the non-constant height along the panel, causing lowered stiffness. In an effort to introduce this into the numerical model, a small perturbation is given to the top and bottom nodes of the sandwich panel. This causes a varying height of the panel and also a slightly lowered stiffness, which is observed in Figure 18. It should be noted that the same mesh size used for the shell elements of the unit cell is used for the numerical model of the sandwich panel. This is done even though it is found that for some deformation states the shell elements, with a mesh size of 1 mm, do not produce proper results. This is motivated by the fact that the shell only differed slightly when determining Young's moduli. Since bending stiffness is mainly dependent on the height of the plate and Young's moduli, this shell mesh is deemed good enough for the case of bending. Also, from the point of practicality it is cumbersome to handle a model of the sandwich panel with five solid elements through the thickness causing the computational time to increase drastically. Finally, since the numerical sandwich panel agreed well with experiments this assumption is deemed valid.

The results obtained from the homogenization of the sandwich panel is presented and compared to the reference model in Figure 19. The stiffness is captured well with the two approaches. It is only for larger displacements that the modeling, using *PART_COMPOSITE, gives a stiffer response. This may be due to the fact that this

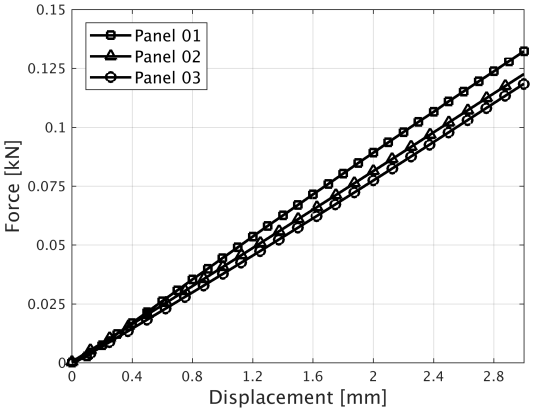

Figure 17: Data obtained from experimental three point bend of three different panels with core of Type A.

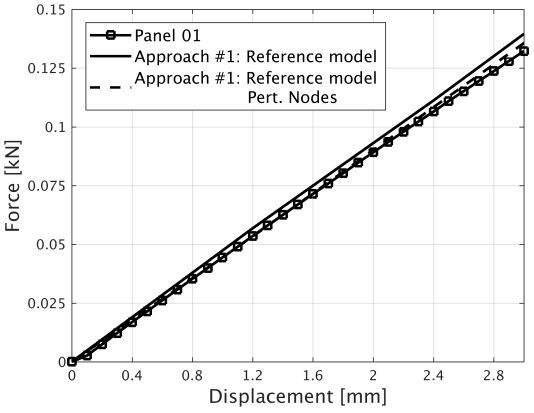

Figure 18: Response of Panel 01 is compared to the numerical model.

approach does not allow the core to collapse and thereby a stiffer response is obtained for larger displacements.

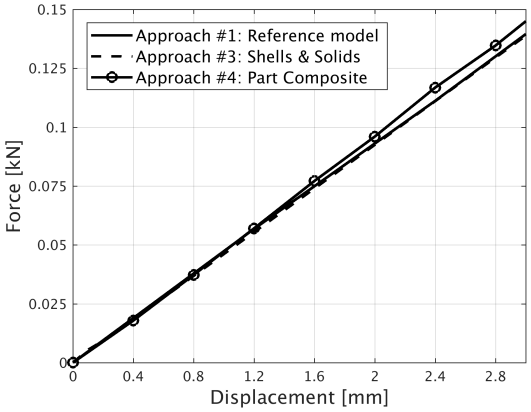

Figure 19: Response from the homogenized modeling approaches are compared to the reference model.

Table 4: Elastic constants obtained from the unit cell of the Type B core. For the shell elements a mesh size of 1 mm was used, and for the solids 9 cubic elements through the thickness was utlized.

	E_x [GPa]	E_z [GPa]	G_{xy}[GPa]	G_{xz}[GPa]	ν_{xy}	ν_{zx}
Shells	12.44	0.062	1.55	0.63		
Solids	9.01	0.033	1.00	0.3		
Difference	38.07%	87.88%	55.00%	110%		

7.3 Homogenization procedure - Type B

In the current section the elastic constants of the Type B core is presented. The approach is equivalent to what is presented for the Type A unit cell. The obtained data is presented in Table 4.

7.4 Three-point bending - Type B

The reference model for the Type B core is compared to the results from the two approaches of modeling the homogenized core, see Figure 20. Unlike the Type A core, the response of the reference model is stiffer that the homogenized model based on solids and shells. This is not unexpected since the difference in response between shell elements and solid elements is greater for the Type B core as compared to the Type A core. The stiffer response could therefore originate from the fact that the shell elements did not represent the Type B core in a proper manner, thus causing a too stiff response. Solid elements with up to 12 elements through the thickness are utilized for the characterization process, so the elastic constants presented in Table 4, should be very close to the

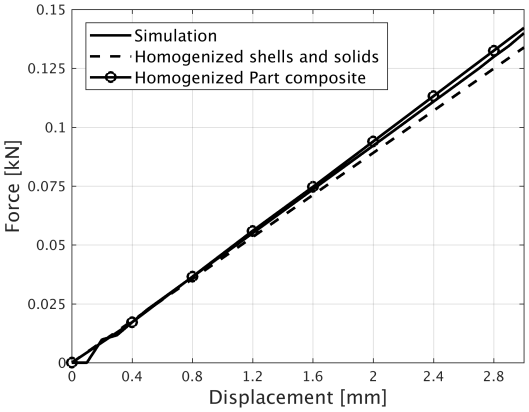

Figure 20: Response from the homogenized modeling approaches are compared to the reference model.

true values. Therefore, the homogenized model based on solid and shell elements should be able to produce a response close to the true response, which is the case for the Type A core.

7.5 Comparing stiffness

In order to illustrate the benefits of the structures presented in this work, the force-displacement response from the Type A and Type B sandwiches are compared to two additional panels. The two additional panels consists of solid steel sheets, based on boron steel. The additional panels are given the equivalent weight or stiffness of Type A and Type B. It is found that to achieve an equivalent stiffness to that of the sandwich panel with a Type A (or Type B) core, a solid plate would require a thickness of 2.925 mm. The weight of such a panel is 750 grams compared to approximately 296 grams for the sandwiches. Figure 21 also contains the response of a solid sheet with equivalent weight to that of the sandwich panel. The stiffness of the sandwich panel is superior.

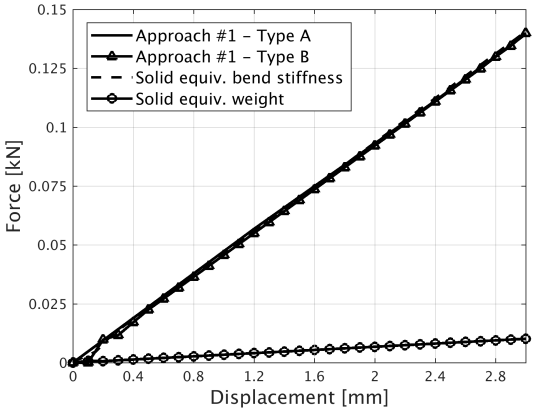

Figure 21: The sandwich with a Type A core is compared to two solid panels. One has equivalent mass to the Type A sandwich. The other one has its equivalent bending stiffness.

8 General discussion

In this work a homogenization procedure has been successfully utilized to predict structural stiffness of sandwich panels. The homogenization process was designed only to predict elastic stiffness for small deformations, thus plasticity and geometrical distortion are not taken into consideration. In order to show the benefits of the panels presented in this work two additional numerical models were created. The first consisted of a panel with equivalent stiffness to that of the Type A sandwich panel and the second consisted of a panel with the Type A sandwich's equivalent weight. It was found that the panels suggested in this work were superior, with respect to stiffness per unit weight.

It was found that for both types of cores, Type A and B, shell elements tended to generate a too stiff response for certain states of deformation. By switching to solid elements for the characterization step of the homogenization process, this issue was addressed. Shell elements was still utilized for the three point bending simulations due to the vast amount of elements that would be required if solids had been used instead. This decision was also motivated by the fact that the predicted Young's modulus by the shell elements only differed slightly compared to the results from the solid elements for the Type A core. Since bending stiffness is mainly dependent on the height of the panel and Young's modulus shell elements were utilized.

However, for Type B the difference in response between shells and solids was greater. The reference model of Approach #1 produced a slightly stiffer response than the homogenized model of Approach #3. Since the error in Approach #3 has been reduced by the characterization process, it should predict stiffness with high accuracy. This was also the case for the Type A core. Finaly, since the difference between Approach #1 and Approach #3 was small, shell elements should also be sufficient for predicting the

Table 5: The number of elements is compared for the full model of the panel, Approach #1, and the two methods for modeling of the homogenized panel, Approach #3 and Approach #4. Reduction in computational time is also presented.

	Approach #1	Approach #3	Approach #4
Number of elements	93 744	17 280	864
Computational time	100%	18%	1%

stiffness of panels based on the Type B core, when subjected to three-point bending.

Lastly, it should be mentioned that the computational times were reduced drastically by the implemented homogenization procedure applied in the present work. The reduction of both the number of elements and computational time is presented in Table 5.

9 Conclusions

A sandwich panel with a core which resembles a three dimensional sinusoidal wave has been investigated with respect to structural stiffness. Due to the geometric complexity of the core a large amount of finite elements was required for the discretization of the panel which would be computationally expensive. In order to reduce both the number of finite element and the computational time a homogenization procedure was suggested where the core was replaced by an equivalent material. The equivalent material should have equal properties to those of the core with respect to structural stiffness.

Two approaches were suggested with respect to modeling of the homogenized panel. The initial approach modeled the core with solid elements using a material model in which the six elastic constants can be set individually. The second approach adopted a shell element for the entire panel and the materials and properties are defined at each, through the thickness, integration point.

Initially a numerical model was created of a sandwich panel when subjected to three point bending. This was validated against experiments and it was found that the numerical results and the experimental results agreed well. To verify the reduction in computational cost the homogenized sandwich panel was also subjected to three-point-bending. It was found that a drastic reduction in computational time was achieved. Furthermore, the stiffness response obtained from the sandwich panels was also compared to the stiffness predicted by the homogenized panels and the results agreed well.

It has been proven that it was possible to model bidirectional sandwich panels in an efficient manner with respect to computational power and accuracy. This makes it possible to incorporate such panels into larger finite element models while keeping the necessary computational time at a decent level. Furthermore, it was concluded that the panel could be utilized for structural stiffness applications where plasticity was not of interest. The homogenization procedure utilized in the current work thus provides

accurate and valid results for stiffness applications where plasticity was not of interest.

10 Acknowledgments

The authors want to thank Mr. Jan Granström for assistance and expertise during the experimental work. Economic support is supplied through the Swedish lightweight innovation programme - LIGHTer, which is gratefully acknowledged.

References

Aktay, L., A.F. Johnson, and B.H. Kröplin (2008). Numerical modelling of honeycomb core crush behaviour. *Engineering Fracture Mechanics* 75.9, pp. 2616–2630.

Bartl, F., H. Klaus, R. Dallner, and O. Huber (2009). Material behaviour of a cellular composite undergoing large deformations. *International Journal of Impact Engineering* 36.5, pp. 667–679.

Bartolozzi, G., M. Pierini, U. Orrenius, and N. Baldanzini (2013). An equivalent material formulation for sinusoidal corrugated cores of structural sandwich panels. *Composite Structures* 100, pp. 173–185.

Besse, C.C. and D. Mohr (2012). Optimization of the Effective Shear Properties of a Bidirectionally Corrugated Sandwich Core Structure. *Journal of Applied Mechanics* 80.1, p. 011012.

Biancolini, M.E. (2005). Evaluation of equivalent stiffness properties of corrugated board. *Composite Structures* 69.3, pp. 322–328.

Chomphan, S. and M. Leekitwattana (2011). Finite Element Study of the Stress Response of Bi-Directional Corrugated-Strip Core Sandwich Beam Suphattharachai Chomphan and 2 Manit Leekitwattana Department of Electrical Engineering , Faculty of Engineering at Si Racha , Department of Naval Architectu. 7.9, pp. 1335–1337.

Deshpande, V.S. and N.A. Fleck (2000). Isotropic constitutive models for metallic foams. *Journal of the Mechanics and Physics of Solids* 48.6, pp. 1253–1283.

Erhart, T. (2011). *Review of Solid Element Formulations in LS-DYNA*.

Kress, G. and M. Winkler (2010). Corrugated laminate homogenization model. *Composite Structures* 92.3, pp. 795–810.

Liu, Q. and G. Subhash (2004). A phenomenological constitutive model for foams under large deformations. *Polymer Engineering and Science* 44.3, pp. 463–473.

Liu, Q., G. Subhash, and X.L. Gao (2005). A parametric study on crushability of open-cell structural polymeric foams. *Journal of Porous Materials* 12.3, pp. 233–248.

Mapelli, C., D. Mombelli, A. Gruttadauria, S. Barella, and E.M. Castrodeza (2013). Performance of stainless steel foams produced by infiltration casting techniques. *Journal of Materials Processing Technology* 213, pp. 1846–1854.

Marek, A. and T. Garbowski (2015). Homogenization of sandwich panels. *Computer Assisted Methods in Engineering and Science*, pp. 39–50.

Nayak, S.K., A.K. Singh, A.D. Belegundu, and C.F. Yen (2013). Process for design optimization of honeycomb core sandwich panels for blast load mitigation, pp. 749–763.

Park, C. and S. Nutt (2000). PM synthesis and properties of steel foams. *Materials Science and Engineering: A* 288.1, pp. 111–118.

Reyes, A., O.S. Hopperstad, T. Berstad, A.G. Hanssen, and M. Langseth (2003). Constitutive modeling of aluminum foam including fracture and statistical variation of density. *European Journal of Mechanics, A/Solids* 22.6, pp. 815–835.

Smith, B., S. Szyniszewski, J. Hajjar, B. Schafer, and S. Arwade (2012). Steel foam for structures: A review of applications, manufacturing and material properties. *Journal of Constructional Steel Research* 71, pp. 1–10.

Szyniszewski, S., B. Smith, J. Hajjar, B. Schafer, and S. Arwade (2014). The mechanical properties and modeling of a sintered hollow sphere steel foam. *Materials & Design* 54, pp. 1083–1094.

Xia, Y., M.I. Friswell, and E.I. Saavedra Flores (2012). Equivalent models of corrugated panels. *International Journal of Solids and Structures* 49, pp. 1453–1462.

Zhang, Y., G. Sun, X. Xu, G. Li, X. Huang, J. Shen, and Q. Li (2013). Identification of material parameters for aluminum foam at high strain rate. *Computational Materials Science* 74, pp. 65–74.

Zupan, M., C. Chen, and N.A. Fleck (2003). The plastic collapse and energy absorption capacity of egg-box panels. *International Journal of Mechanical Sciences* 45.5, pp. 851–871.

Paper B

Evaluation of perforated sandwich cores for crash applications

Authors:
Samuel Hammarberg, Jörgen Kajberg, Göran Lindkvist, Pär Jonsén

To be submitted.

Evaluation of perforated sandwich cores for crash applications

Samuel Hammarberg, Jörgen Kajberg, Göran Lindkvist, Pär Jonsén

Abstract

Legislations force the vehicle industry to reduce greenhouse gas emissions. Introducing lightweight components, with maintained performance, into the body in white is one contribution to achieve this goal. The present work suggests lightweight boron steel sandwiches with perforated cores for energy absorption applications to address this issue. Hat profile geometries, subjected to crushing, are adopted to investigate energy absorption properties. The energy absorbed by the sandwich is compared to a solid steel sheet hat profile with equivalent weight. It is found that the specific energy absorption properties have been increased through the introduction of the sandwich structures. The findings suggests the possibility to reduce vehicle weight by incorporation of sandwich hat profiles based on perforated cores.

1 Introduction

Legislation regarding green house gas emissions force vehicle manufacturers to bring forth new and innovative solutions. These solutions may refer to more efficient engines and lighter components of the vehicle's body in white (BIW).

Methods for reducing vehicle weight have been developed over the last decades. In the 1970's, press hardening was invented by the former SSAB HardTech, now Gestamp HardTech, resulting in increased performance of steel, reducing the weight of the BIW. As the first automotive manufacturer, Saab Automobile implemented such components in the 1980's. Further development of press hardening made it possible to manufacture components with with tailored properties by adjusting the thermal history in areas where soft zones are desired, further reducing the weight (Oldenburg and Lindkvist, 2011).

An additional method for reducing vehicle weight is incorporation of sandwich structures into the BIW. A typical sandwich consists of stiff face plates separated by a light weight core. The ideal core has the lowest possible weight with sufficient stiffness to withstand transverse and shear loads, maintaining the initial distance between the face plates. A wide range of cores exist, such as foams, geometrical patterns, and solid cores.

In Gibson and Ashby, 1999 it was shown that the mechanical properties of foams are strongly influenced by the bulk material of the foam. Thus, the selection of bulk material is of importance when the foam is selected. Smith et al., 2012 has presented a review on steel foam, including manufacturing processes and structural applications. Additional work has been performed by Park and Nutt, 2000, where steel foam was manufactured

and found to have substantial specific energy absorption properties. The manufacturing method was deemed simple and affordable for small to mid sized components. In Szyniszewski, Smith, Arwade, et al., 2012, a Desphande-Fleck constitutive model was utilized to model the triaxial behavior of steel foam. After calibration, the constitutive model results comparable to experimental data. Further work on modeling of steel foam was conducted in Szyniszewski, Smith, Hajjar, et al., 2014. A lot of work has also been done on aluminum foam, see for instance Sulong et al., 2014 and Marsavina et al., 2016, which is a suitable choice for imporving crashworthiness Zhang et al., 2013. Özer et al., 2017 utilized a sandwich structure for crash applications. A crash box was generated with a core based on syntactic foam which proved beneficial with respect to energy absorption. In the work conducted by Xiao et al., 2015 crashworthiness was investigated for a foam filled bumper beam. It was found that utilizing functionally lateral graded foam within the bumper beam was beneficial with respect to energy absorption. Thus, it can be found that several candidates for bulk material are available. However, mixing materials may cause some difficulties during recycling when the materials must be separated. Thus, from that point of view, it may be beneficial to manufacture homogeneous components with respect to the included materials.

Adopting geometrical patterns has been done by Aktay et al., 2008 where the crush behavior of honeycomb was studied both experimentally and numerically. Nayak et al., 2013 utlized honecomb sandwich panels, which were designed for optimal blast load mitigation. Additional work on such geometries was carried by Sun et al., 2017. The studdy contributes to increase the knowledge of crashworthiness and collapse modes of the aforementioned type of core. Honeycomb patters were also studied by Wu et al., 2017, where varies honeycomb geometries were investigated at low impact velocities. The core consisted of aluminum whereas carbon reinforced polymer (CFRP) was used as face plates, which was compared to a panel solely based on CFRP. The increased performance of the sandwich was evident. A variation of a geometrical pattern for core, was used by Mohr and Wierzbicki, 2005, and consists of a perforated steel plate, where box columns were subjected to a axial loading.

The present work suggests a lightweight sandwich structure with a perforated core, similar to that of Mohr and Wierzbicki, 2005, for energy absorption applications. The aim is to reduce weight while maintaining crashworthiness. Weight is reduced due to the hole pattern, which is carefully placed in order to maintain performance. In contrast to several of the aforementioned works, the sandwich is homogeneous with respect to material through the thickness, i.e. both face plates and core consist of hardened boron steel, 22MnB5. A geometry in the shape of a hat profile is selected, resembling a simplified beam section of the BIW. In order to evaluate energy absorption capacity, experiments and numerical simulations are adopted.

For crash applications, the energy should be absorbed in a controlled manner and the peak force must not exceed a critical value to ensure passenger safety. Therefore, force-displacement response and the amount of energy absorbed are studied experimentally and numerically. Strain rate effects are not included in the present work.

In the experiment, the hat profile is subjected to crash loading in the form of a barrier.

Force and load line displacement are gathered. The experiment is recreated numerically to ensure the robustness of the numerical model. With a robust numerical representation of the hat profile, various hole sizes are tested numerically in order to investigate the effect on the force-displacement response.

The response of the sandwich hat profile, is compared to a reference model based on a solid sheet with an equivalent weight. To show the benefits of a sandwich structure, an additional reference model is created, consisting of a perforated sandwich with the same thickness as the lightweight sandwich but with holes through both core and outer sheets.

2 Geometries and materials

In the current section, the purpose is to introduce the geometries studied in the present work. This is followed by a presentation of the material data, where the manufacturing process for joining the layers of the sandwich is presented.

2.1 Geometries

Hat profiles, subjected to crash loading, are studied in the present work. In particular, three types of hat profiles are used:

- Type A - Hat profile based on a sandwich with a perforated core.
- Type B - Reference hat profile based on a solid sheet with equivalent weight to Type A.
- Type C - Reference hat profile based on a perforated sandwich with holes through both core and outer sheets.

Type A consists of a core with a thickness of 1.232 millimeters and face plates with a thickness of 0.308 millimeters. Further dimensions of the Type A hat profile are presented in Figure 1. Type B consists of a solid steel sheet, 1.61 millimeters thick, with equivalent weight and curvature of type A. This is a reference geometry to see how the specific energy absorption is affected. Type C consists of a perforated steel sheet, with a hole pattern, thickness and curvature equal to Type A. Type C is used to see how the lack solid face plates affects the energy absorption.

Three different hole diameters are used for the Type A hat profile: 3 mm, 2 mm, and 1 mm respectively. For each core the hole size is kept constant. A generic illustration of the hole distribution is presented in Figure 2. In each row and column the holes are distributed with a distance of $2D$, where D is the hole diameter. The next row is given an offset of D, in the direction of the width, to its two neighboring rows. It should be mentioned that no holes were placed over the radius of the hat profile, as this would drastically reduce its capacity to absorb energy.

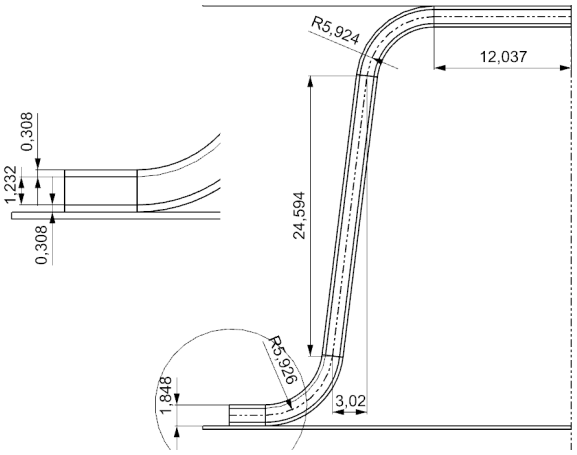

Figure 1: Hat profile geometry with dimensions given in millimeters. The geometry is used for evaluation of the sandwiches in energy absorption applications.

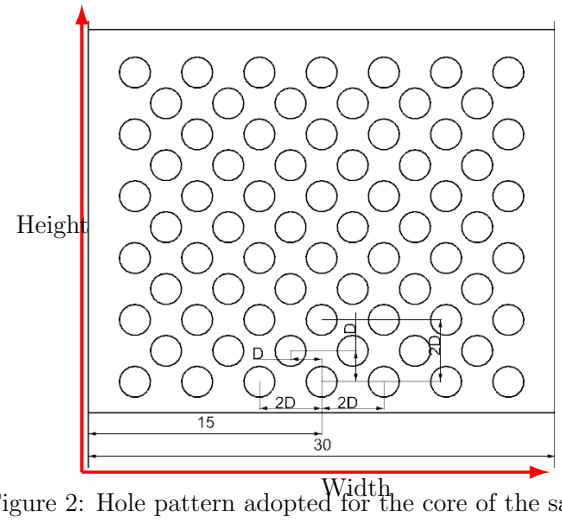

Figure 2: Hole pattern adopted for the core of the sandwich.

Figure 3: From the rolling process it was found that grains had formed over the boundaries between face plates and core in the sandwich. Courtesy of Lars Wikström at Gestamp Hardtech, Luleå.

2.2 Material and manufacturing

The sandwich consists of hardened boron steel, 22MnB5. Manufacturing of the sandwich is carried out by drilling holes in the core, which are distributed according to Figure 2. The core and face plates are joined by a hot-rolling process to ensure grain formation over the interface between face plates and core, see Figure 3. Thus a strong bond exists between the layers of the sandwich, which is of importance to reduce the possibility of delamination between face plates and core. After hot-rolling, the geometry of a hat profile is obtained by hot stamping.

3 Modeling

The present section focuses on the numerical modeling. The multi-physics, explicit solver LS-DYNA R10 was utilized, to evaluate performance of the hat profiles.

The numerical model consists of three parts: hat-profile, punch, and support. This is presented in Figure 5. It should be noted that for the hat profile of Type A, three subparts make up the sandwich which consisting of two face plates and a core. A symmetry condition is applied to reduce the number of finite elements, thus reducing computational time. Discretization is performed using five under-integrated solid elements (ELFORM = 1 within LS-DYNA), through the thickness. Hourglass stabilization is added, ensuring hourglass energy is kept below 10 % of the internal energy. Strain rates are not taken into account, therefore the punch shown in Figure 5 is given a prescribed constant acceleration of 6 mm/s^2, in order to reduce computational time. Termination time is set to 100 ms, resulting in a final velocity of 0.6 m/s for the punch. To reproduce the experimental set up the bottom left nodes of the hat profile are fixed in all translations and rotations. Contacts are handle by an automatic single surface contact algorithm with pinball segment based contact triggered. In the contact, static and dynamic friction coefficients are set to 0.3. Adhesion between face plates and core is handle by allowing the core and face plates to

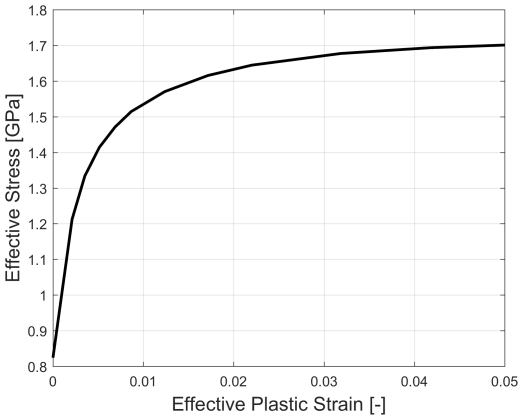

Figure 4: Effective stress (von Mises) vs effective plastic strain for hardened boron steel 22MnB5.

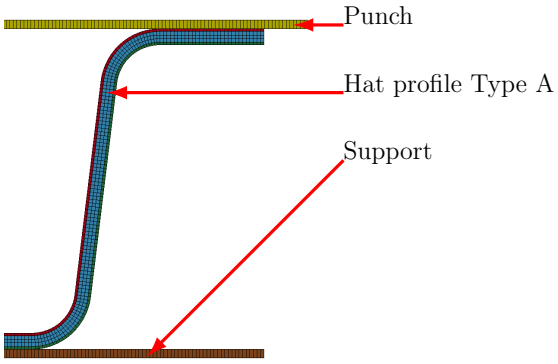

Figure 5: Hat profile of Type A with a perforated core with 3 millimeter holes. The bottom left flange is fully fixed to represent the experimental setup.

share nodes. This is motivated by the fact that grains form over the boundaries due to the hot rolling process utilized for joining the core and face plates, see Figure 3.

The punch and support are assumed to be much stiffer than the hat profile. Thus, it is suitable to approximate the punch and support as rigid bodies in the numerical model. The mechanical properties of the hat profile are represented by a piece-wise linear plasticity model, with the quasi-static stress-strain response according to Figure 4.It should me noted that strain rate effects are not taken into account. Density, Young's modulus and Poisson's ratio are 7850 kg/m^3, 206 GPa and 0.3 respectively.

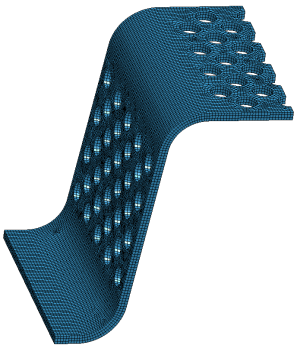

Figure 6: Core of the Type A hat profile with 3 millimeter holes.

4 Results and Discussion

In the current section the results from the experiments and the numerical models are presented and discussed.

4.1 Numerical model

Three different numerical models are created: Type A, Type B and Type C. Type B and C are reference models used to compare to the response from Type A. Three versions of perforated cores are created, with holes diameters set to 1, 2 and 3 mm respectively. For the Type A sandwich with hole diameter of 3 mm, three states of deformation are presented in Figure 7, with the von Mises stress presented.

The force-displacement response from the three versions of Type A is presented in Figure 8. No real effect, caused by the difference in hole size, is found. The difference in weight is insignificant: a diameter of 1 mm results in a weight 211 g, whereas the cores with hole diameter of 2 and 3 mm both give a weight of 215 g. This is a total difference of less than 2 %. Thus, the choice of hole diameter should come down to which application is considered. If the plates are to be joined with some rolling procedure, smaller holes may be beneficial in order to reduce intrusion of the skins into the holes of the perforated core.

In Figure 9, the response from Type A is compared to the reference models Type B and Type C. It is seen that the three types of cores produce similar response curves, with the only difference being the magnitude of the force and thereby the area under the curve. Type A absorbs approximately 20 % more than Type B, and 50 % more than Type C. This indicates that the Type A sandwich has an increased specific energy absorption capability as compared to a solid sheet of equivalent weight. Additionally, by comparing the Type A sandwich, to the Type C perforated plate it is clear that it is the sandwich properties which contributes to the enhanced properties and not only the increased thickness.

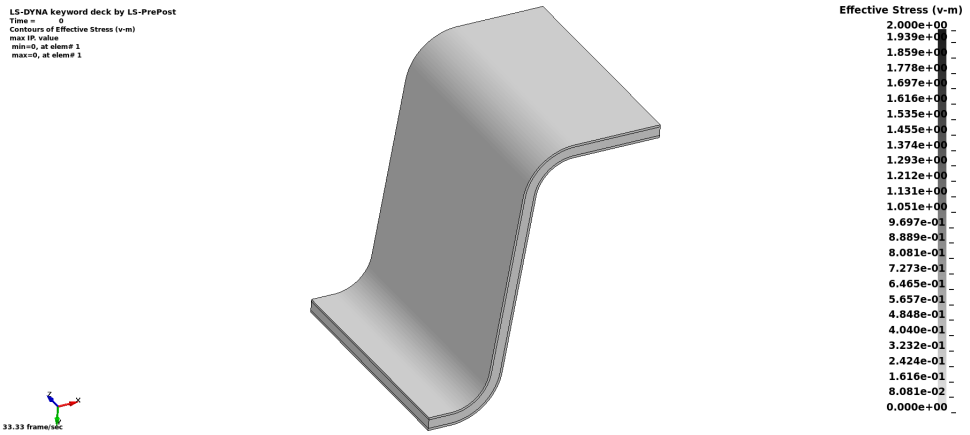

(a) Start at T=0 ms

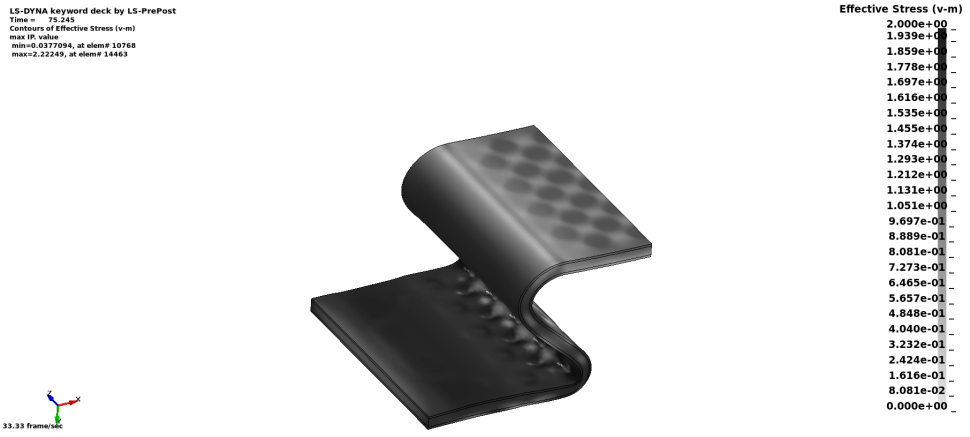

(b) Middle at T=86 ms

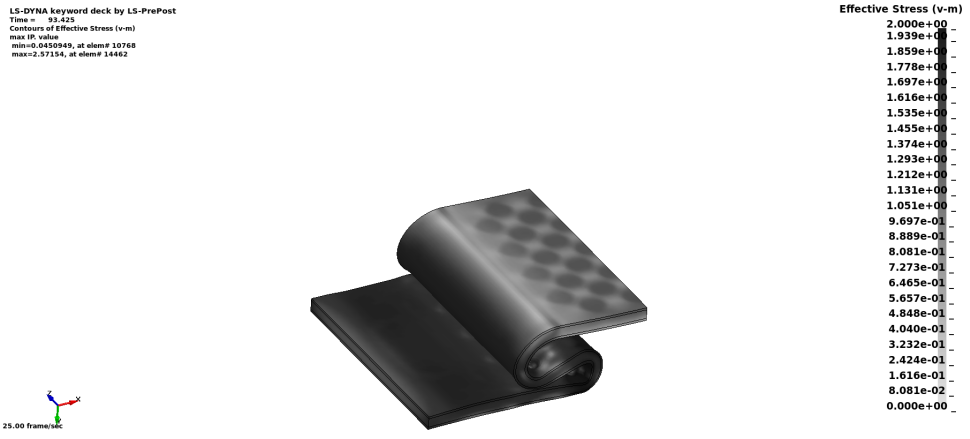

(c) End of simulation

Figure 7: Type A hat profile during deformation, with the fringe plot of the von Mises stress.

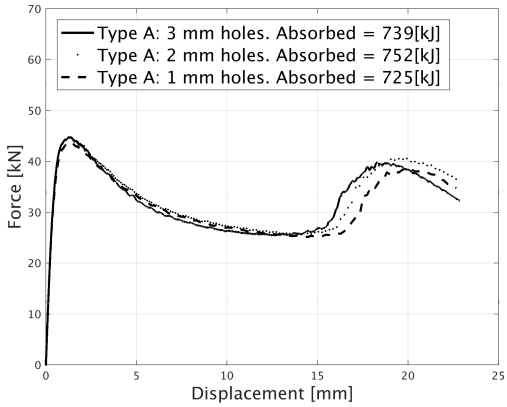

Figure 8: A comparison between the Type A hat profile when the hole size of the perforated core is varied. The response remain quite similar.

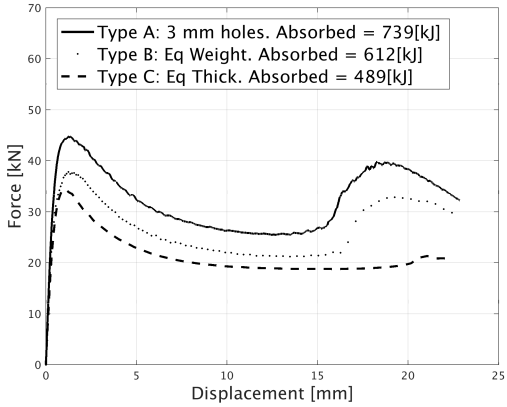

Figure 9: Type A with a perforated core with 3 millimeters holes is compared to Type B and Type C. Type B refers to a hat profile of equivalent weight to Type A. Type C refers to a hat profile based on a perforated plate with 3 millimeter holes and equivalent thickness of Type A.

5 Conclusions

Legislation is forcing the vehicle industry to reduce its greenhouse gas emissions. A way to partly achieve this, is reducing weight of vehicle components. The present work suggests a lightweight hardened boron steel sandwich concept, with a perforated core. The perforated core contains a hole distribution which should be adapted for a given application.

In the present study a hat profile was selected in order to investigate the potential of the sandwich concept. Thus no holes were placed over the radius. A total of three different hole sizes were investigated, which proved to generate similar response.

To quantify the performance of the sandwich (Type A), a comparison was made to a solid hat profile of equivalent weight (Type B). It was found that Type A possessed superior energy absorption capacity compared to Type B. Additionally, to confirm that it was the sandwich structure which contributed to the enhanced response, and not just the difference in thickness between Type A and Type B, an additional hat profile was tested (Type C), solely consisting of a perforated core with the equivalent thickness to Type A. Again, the superior properties of Type A were evident.

Thus, it seems like the Type A sandwich is a promising, lightweight concept for energy absorption applications.

6 Acknowledgment

The authors want to thank Gestamp HardTech and Swerea Mefos for assistance and expertise during the experimental work. Economic support is supplied through the Swedish lightweight innovation programme - LIGHTer, which is gratefully acknowledged.

References

Aktay, L., A.F. Johnson, and B.H. Kröplin (2008). Numerical modelling of honeycomb core crush behaviour. *Engineering Fracture Mechanics* 75.9, pp. 2616–2630.

Gibson, L. and M. Ashby (1999). *Cellular Solids - Structure and Properties - Second edition*. 2nd. Cambridge University Press (2nd edition).

Marsavina, L., J. Kováčik, and E. Linul (2016). Experimental validation of micromechanical models for brittle aluminium alloy foam. *Theoretical and Applied Fracture Mechanics* 83, pp. 11–18.

Mohr, D. and T. Wierzbicki (2005). On the Crashworthiness of Shear-Rigid Sandwich Structures. *Journal of Applied Mechanics* 73.4, pp. 633–641.

Nayak, S.K., A.K. Singh, A.D. Belegundu, and C.F. Yen (2013). Process for design optimization of honeycomb core sandwich panels for blast load mitigation, pp. 749–763.

Oldenburg, M. and G. Lindkvist (2011). Tool thermal conditions for tailored material properties. *HTM - Haerterei-Technische Mitteilungen* 66.6, pp. 329–334.

Özer, H., Y. Can, and M. Yazıcı (2017). Investigation of the Crash Boxes Light Weighting with Syntactic Foams by the Finite Element Analysis. *Acta Physica Polonica A* 132.3, pp. 734–737.

Park, C. and S. Nutt (2000). PM synthesis and properties of steel foams. *Materials Science and Engineering: A* 288.1, pp. 111–118.

Smith, B., S. Szyniszewski, J. Hajjar, B. Schafer, and S. Arwade (2012). Steel foam for structures: A review of applications, manufacturing and material properties. *Journal of Constructional Steel Research* 71, pp. 1–10.

Sulong, M.A., M. Vesenjak, I.V. Belova, G.E. Murch, and T. Fiedler (2014). Compressive properties of Advanced Pore Morphology (APM) foam elements. *Materials Science and Engineering: A* 607, pp. 498–504.

Sun, G., X. Huo, D. Chen, and Q. Li (2017). Experimental and numerical study on honeycomb sandwich panels under bending and in-panel compression. *Materials & Design* 133, pp. 154–168.

Szyniszewski, S., B. Smith, J. Hajjar, B. Schafer, and S. Arwade (2014). The mechanical properties and modeling of a sintered hollow sphere steel foam. *Materials & Design* 54, pp. 1083–1094.

Szyniszewski, S., B. Smith, S. Arwade, J. Hajjar, and S. Benjamin (2012). Tensile and shear element erosion in metal foams. *12th International LS-DYNA Users Conference* 1, pp. 1–10.

Wu, Y., Q. Liu, J. Fu, Q. Li, and D. Hui (2017). Dynamic crash responses of bio-inspired aluminum honeycomb sandwich structures with CFRP panels.

Xiao, Z., J. Fang, G. Sun, and Q. Li (2015). Crashworthiness design for functionally graded foam-filled bumper beam. *Advances in Engineering Software* 85, pp. 81–95.

Zhang, Y., G. Sun, X. Xu, G. Li, X. Huang, J. Shen, and Q. Li (2013). Identification of material parameters for aluminum foam at high strain rate. *Computational Materials Science* 74, pp. 65–74.